ECOLOGICAL GENOMICS

Genomic architecture of a genetically assimilated seasonal color pattern

Karin R. L. van der Burg[1]*, James J. Lewis[1,2], Benjamin J. Brack[1], Richard A. Fandino[1], Anyi Mazo-Vargas[1], Robert D. Reed[1]*

Developmental plasticity allows genomes to encode multiple distinct phenotypes that can be differentially manifested in response to environmental cues. Alternative plastic phenotypes can be selected through a process called genetic assimilation, although the mechanisms are still poorly understood. We assimilated a seasonal wing color phenotype in a naturally plastic population of butterflies (*Junonia coenia*) and characterized three responsible genes. Endocrine assays and chromatin accessibility and conformation analyses showed that the transition of wing coloration from an environmentally determined trait to a predominantly genetic trait occurred through selection for regulatory alleles of downstream wing-patterning genes. This mode of genetic evolution is likely favored by selection because it allows tissue- and trait-specific tuning of reaction norms without affecting core cue detection or transduction mechanisms.

Developmental plasticity—the ability of one genotype to produce alternative phenotypes in response to environmental cues—is an important driver of phenotypic diversity (*1*, *2*). Because plasticity allows genomes to encode different potential phenotypes, it can be a source of phenotypic variation that natural selection can act upon (*3*). Waddington coined the term "genetic assimilation" to describe a reduction of plasticity, where selection leads to expression of an ancestrally conditional phenotype in the absence of the original environmental cue (*4*). Little is currently known, however, about the genetic mechanisms that underlie the assimilation of ancestrally plastic phenotypes (*5*).

We sought to characterize the genomic architecture of genetic assimilation using seasonal wing color plasticity in the common buckeye butterfly *Junonia coenia*, which develops a pale tan wing color under warm, long-day conditions, and a dark red color under cold, short-day conditions (Fig. 1A) (*6*). The wing color reaction norm can evolve through both artificial and natural selection, and both tan and red phenotypes are fixed in some populations and closely related species (*7*, *8*).

To isolate alleles that control wing color plasticity, we generated two artificial selection lines for increased and reduced wing color plasticity, respectively. Butterflies selected for increased plasticity (the "Plastic" line) were subjected to Waddington's alternating selection regime (*9*): When reared under warm, long-day conditions, the palest butterflies were selected to breed, after which offspring were reared under cool, short-day conditions, and the reddest butterflies were selected. Within six generations, the color difference between warm- and cold-reared animals increased (Fig. 1B and fig. S1), and the reaction norm slope increased accordingly (Fig. 1, C and D, and table S1). Selection for reduced wing color plasticity (the "Red" line) was achieved by rearing offspring under warm conditions and selecting the reddest butterflies each generation. After 12 generations, the red phenotype became predominant under conditions where butterflies would normally be tan (Fig. 1E and fig. S1), and there was a significant reduction in the reaction norm slope (Fig. 1, C and D, and table S1). Thus, we created a Plastic line in which the red wing phenotype is induced by environmental cues, and a Red line in which the red wing phenotype is assimilated.

Evolution of environmental response should be attributable to changes in one of three mechanisms: (i) cue detection, the capacity to detect differences in the environment; (ii) cue transduction, the translation of a cue into an internal signal such as a hormone titer; and (iii) tissue response, the way a specific tissue responds to the internal signal (*10*). We thus sought to determine to what extent we could explain the plasticity differences between our selection lines through changes in any of these mechanisms.

Wing color plasticity in *J. coenia* is caused by environmentally induced changes in the timing of an ecdysone pulse during early pupal development (*11*). If assimilation of the red phenotype occurred because the ability to detect or transduce cues was lost, we would predict that warm-reared Red line butterflies would have an ecdysone profile similar to that of cold-reared Plastic line butterflies (which are red). However, we found that ecdysone titers in warm-reared butterflies from the Red line were the same as in warm-reared butterflies from the Plastic line (Fig. 1F), which are red and tan, respectively. Ecdysone titers responded to environmental cues similarly in both lines. This indicates that in the genetically assimilated Red line, wings became red despite a normally functioning cue detection and transduction system. Thus, we infer that genetic assimilation of red wing coloration occurred through changes in how wing tissues respond to an otherwise conserved endocrine signal.

To determine the genetic basis of changes in wing color plasticity, we performed F_3 crosses using individuals from the Red and Plastic lines and scored phenotypes of individuals raised under conditions that would normally induce tan phenotypes (i.e., warm, long light cycle). We then selected 20 of the most extreme tan (i.e., environment-responsive) and 21 of the most extreme red (i.e., environment-unresponsive) individuals for whole-genome resequencing (tables S2 and S3). A genome-wide association analysis, using the amount of red color in warm-reared animals to signify reduced plasticity, revealed four genomic loci (Fig. 2A). We identified candidate genes at these loci by comparing hindwing mRNA levels between the Red and Plastic lines at four developmental stages spanning before, during, and after the pupal ecdysone signal that determines wing color (fig. S5A). We detected 13 differentially expressed genes (Wald adjusted $P < 0.05$) within 25 kb of a plasticity-associated nucleotide variant (Fig. 2, B and C), of which the majority were differentially expressed late in development, during pigment synthesis (Fig. 2C).

We next used one of three additional criteria to select a subset of these genes for functional validation: (i) suspected wing-patterning function (*cortex*), (ii) highest expression levels at the differentially expressed stage (*trehalase* and *Dscam3*), or (iii) differential expression across multiple developmental stages (*CG8930*, hereafter *herfst*). We then used CRISPR/Cas9 somatic deletion mosaics (figs. S8 and S9) to test the function of *Dscam3* in the Plastic line, and *cortex*, *trehalase*, and *herfst* in the Red line, consistent with which lines showed elevated expression of the respective targets. We did not observe *Dscam3* phenotypes, but all three genes in the Red line produced distinct mutant clones of tan scales in a background of otherwise normal Red line red scales. These are phenotypes where individual butterflies display wing patterns that are mosaic for both summer and autumn coloration (Fig. 2D). One of the genes, *cortex*, is implicated in wing pattern adaptation in peppered moths and *Heliconius* butterflies (*12*, *13*). The others are

[1]Department of Ecology and Evolutionary Biology, Cornell University, Ithaca, NY, USA. [2]Baker Institute for Animal Health, Cornell University, Ithaca, NY, USA.
*Corresponding author. Email: krv32@cornell.edu (K.R.L.v.d.B.); robertreed@cornell.edu (R.D.R.)

Downloaded from http://science.sciencemag.org/ on November 5, 2020

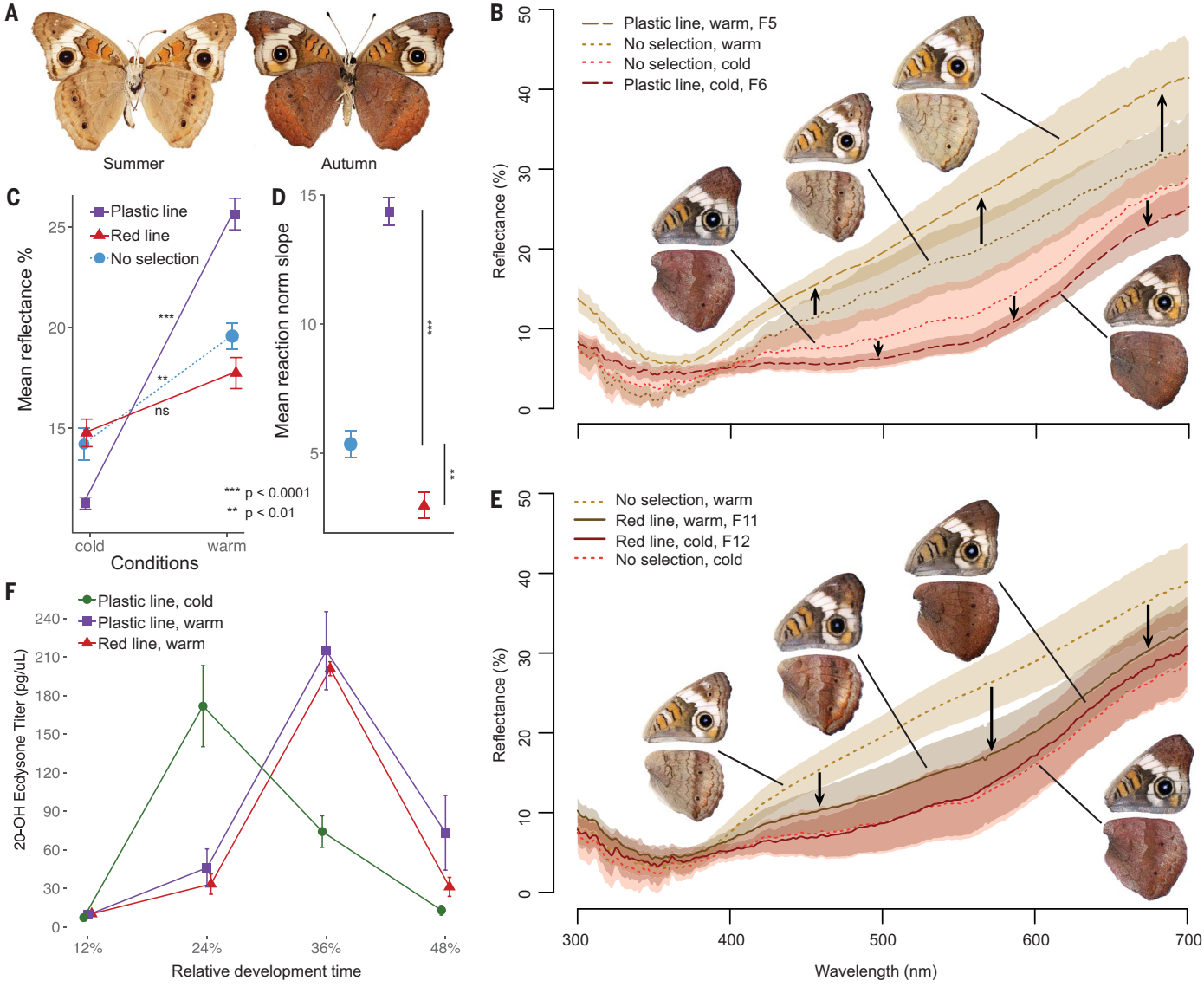

Fig. 1. Rapid selection for increased and reduced plasticity. (**A**) Seasonal morphs of *J. coenia*. (**B**) Wing color response differences after six generations of selection for increased plasticity (warm = 27°C and 16 hours of light, cold = 19°C and 8 hours of light). (**C** and **D**) Wing color reaction norms (C) and slopes (D) differ between selection lines (*t* test *P* values shown). (**E**) Wing color response differences after 12 generations of selection for reduced plasticity. (**F**) 20-hydroxy-ecdysone titers for the different selection lines under different conditions show no difference between warm-reared Plastic line and Red line butterflies. Error bars in (C), (D), and (F) and shaded areas in (B) and (E) denote SD.

trehalase, which encodes an enzyme that converts trehalose into glucose, a constituent of the red wing pigment rhodommatin (*14*), and *herfst*, a previously uncharacterized zinc finger domain gene. In sum, knockouts of three candidate genes showed that each is individually necessary for production of the red autumn phenotype, and the loss of function of any one of them phenocopies the tan summer phenotype.

The evolution of reaction norms might be traceable to differences in regulatory regions that control the responsiveness of a gene to an inductive signal, such as a hormone (*15*). This model is consistent with mRNA expression differences observed between our selection lines, coupled with the lack of protein coding variation. To further characterize the nature of cis-regulatory variation between selection lines, we used ATAC-seq (assay for transposase-accessible chromatin with high-throughput sequencing) to identify active cis-regulatory elements (CREs), and Hi-C chromatin contact mapping to assess physical interactions between CREs and gene promoters (*16*). Genome-wide chromatin accessibility was similar between lines, with only 13% of ATAC-seq peaks differing (Wald adjusted $P < 0.05$), most of which (11%) varied late in development during pigment deposition. Of 64 associated nucleotide variants, 58 were located in presumptive CREs (i.e., within ATAC-seq peaks), whereas only two were nonsynonymous amino acid substitutions.

For *cortex*, ATAC-seq plus Hi-C highlighted a cluster of significant nucleotide variants in the first intron that correspond to a series of nonvariable ATAC-seq peaks that physically interact with the *cortex* promoter (Fig. 3A, fig. S7, and table S9). For *trehalase*, ATAC-seq plus Hi-C revealed a single major ~40-kb upstream CRE varying in accessibility between lines (Wald adjusted $P < 0.05$) with strong promoter interaction during pigment synthesis (Fig. 3B, fig. S7, and table S9), suggesting differences in CRE activity. For *herfst*, ATAC-seq plus Hi-C revealed a hub of interactions where three CREs, including the *herfst* promotor, loop to each other. Two of these elements also showed differences in chromatin accessibility between lines (Wald adjusted $P < 0.05$) (Fig. 3C, fig. S7, and table S9), again suggesting line-specific differences in CRE activity. These results, coupled with

Downloaded from http://science.sciencemag.org/ on November 5, 2020

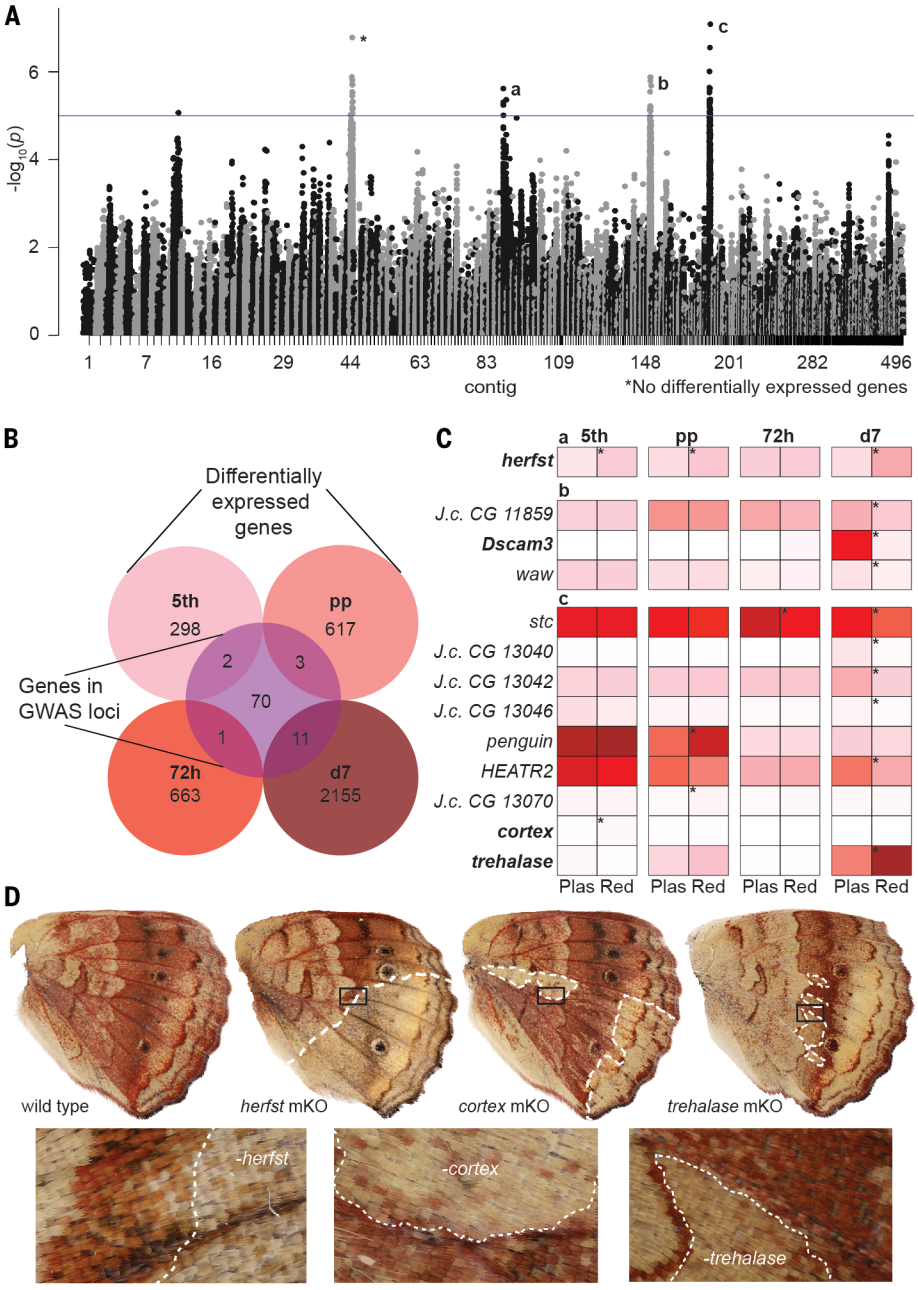

Fig. 2. Three genes underlying reaction norm changes between selection lines. (**A**) Four loci showed multiple nucleotides significantly associated ($P \leq 0.00005$) with red color assimilation in Red line × Plastic line F_3 crosses. Asterisk denotes an associated contig with no differentially expressed genes. (**B**) Differentially expressed genes across multiple stages [fifth instar (5th), pre-pupa (pp), 72 hours after pupation (72h), day 7 after pupation (d7)]. Overlap with center circle indicates genes within 50 kb of an associated nucleotide. GWAS, genome-wide association study. (**C**) Differential expression of candidate genes in Plastic and Red lines. Asterisks denote significance (Wald adjusted $P < 0.05$). Genes selected for functional validation are in bold. Letters a, b, and c correspond to nucleotide association regions shown in (A). (**D**) CRISPR/Cas9 somatic mosaic knockouts (mKO) confirm that *herfst*, *cortex*, and *trehalase* are all required for development of red pigmentation characteristic of the autumn morph.

observed expression differences, sequence associations in CREs, and lack of coding variation, support a model where genetic assimilation of red wing coloration was facilitated by selection on alleles of *cortex*, *trehalase*, and *herfst* with different cis-regulatory functions.

The three genes we identified in this study suggest mechanisms through which assimilation can evolve (Fig. 4). We speculate that *trehalase* plays a direct role in pigment synthesis, and that an environmentally insensitive increase of *trehalase* expression in the Red line promotes production of red pigmentation. It is noteworthy that *trehalase* is also up-regulated in cold-reared *J. coenia* (*17*), which suggests that this gene is involved in generating both the induced and the assimilated red phenotype. In contrast to *trehalase*, differences in *cortex* and *herfst* expression occur during larval development, before the inductive ecdysone pulse (Fig. 4B). These pre-cue expression differences suggest that these genes play an upstream role in how the wing color regulatory network responds to the ecdysone signal. We speculate that early expression of these genes may tune the parameters of ecdysone response—for example, through threshold sensitivity and/or critical period. As with *trehalase*, higher mRNA abundance in the Red line suggests that this occurs through a loss of repression under summer-like conditions. Ultimately, *trehalase*, *cortex*, and *herfst* are all necessary for development of the red autumn morph, and they appear to function at different points in a shared patterning network. Our results indicate that reaction norm variation can be both quantitative and multigenic, and we conjecture that allelic variants of these genes may act additively to shape the reaction norm curve.

Our study shows that seasonal plasticity can evolve rapidly, likely through cis-regulatory changes distributed across multiple downstream trait-specific genes. We propose that this mode of genetic evolution should be favored by selection because it allows tissue- and trait-specific tuning of reaction norms while avoiding broad effects that would otherwise be caused by changes to core seasonal response mechanisms.

Downloaded from http://science.sciencemag.org/ on November 5, 2020

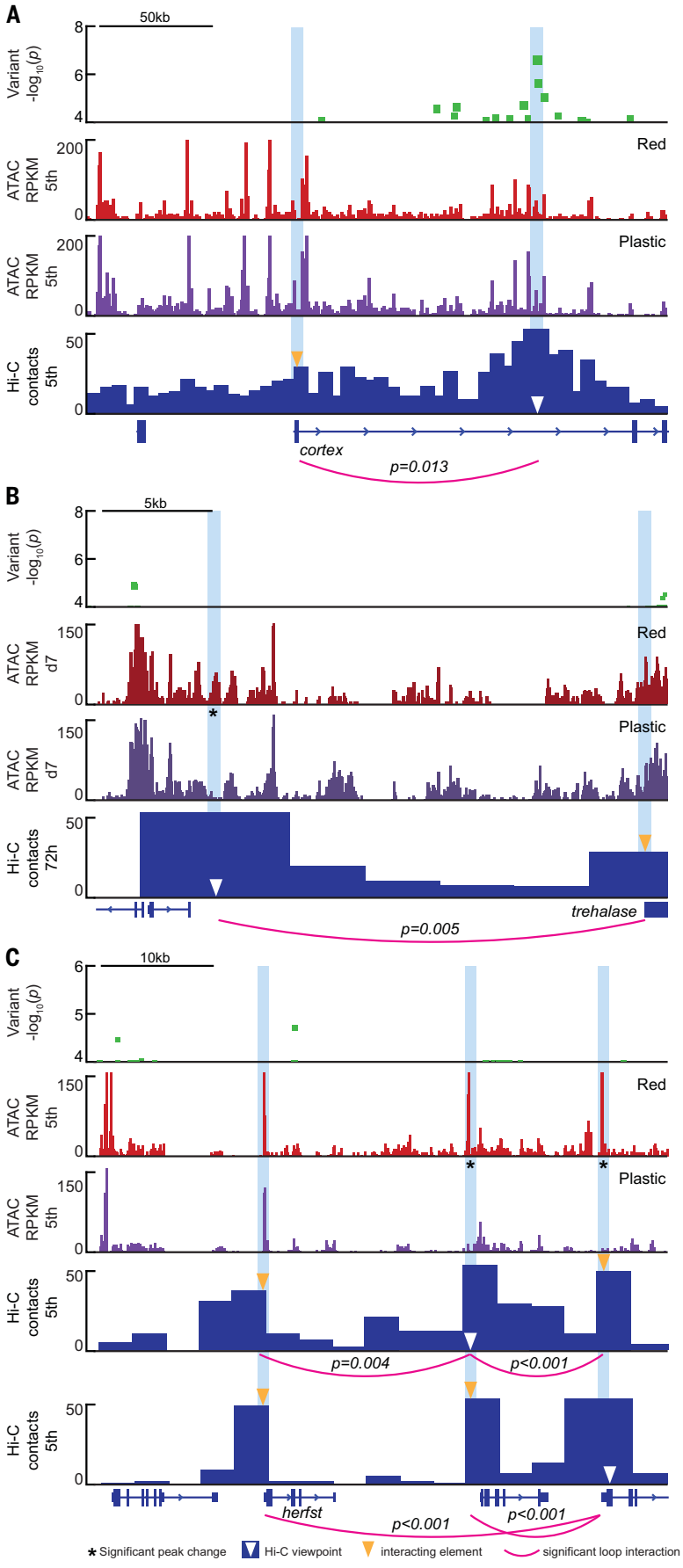

Fig. 3. Selection lines show cis-regulatory variation at causal genes. The plots show nucleotide variants associated with assimilation of red color (green), chromatin accessibility (ATAC-seq) in Red (red) and Plastic (purple) line butterflies, and Hi-C chromatin interactions (blue) using candidate CREs as viewpoints (white triangles). Lines (pink) denote significant CRE-promoter (yellow triangles) interactions, inferred from Hi-C (Fisher's exact test, $P < 0.05$). Asterisks indicate chromatin accessibility differences (Wald adjusted $P < 0.05$). (**A**) In fifth-instar wing discs, CREs under a cluster of significant nucleotide variants interact with the *cortex* promoter. (**B**) In day 7 (d7) pupae, during pigment synthesis, a CRE showing differential accessibility between lines interacts with the *trehalase* promoter. (**C**) In fifth-instar wing discs, there is a three-way chromatin interaction that includes the *herfst* promoter and two CREs that show accessibility differences between lines.

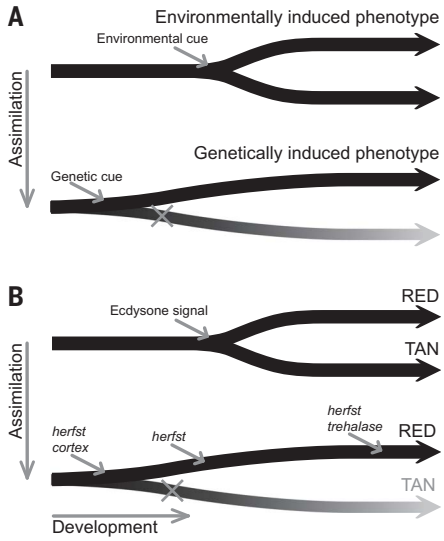

Fig. 4. Multigenic evolution of genetic assimilation. (**A**) Theoretical model where assimilation occurs by the appearance of a genetic cue that replaces the environmental cue to induce a phenotype. (**B**) In *J. coenia*, differential expression of three genes across wing development, independent of endocrine signaling, can underlie the genetic cue through which assimilation of wing color evolves.

REFERENCES AND NOTES

1. D. W. Pfennig *et al.*, *Trends Ecol. Evol.* **25**, 459–467 (2010).
2. R. F. Schneider, A. Meyer, *Mol. Ecol.* **26**, 330–350 (2017).
3. M. J. West-Eberhard, *Developmental Plasticity and Evolution* (Oxford Univ. Press, ed. 1, 2003).
4. C. H. Waddington, *Evolution* **7**, 118–126 (1953).
5. J.-M. Gibert, *Dev. Genes Evol.* **227**, 297–307 (2017).
6. K. C. Smith, *J. Res. Lepid.* **30**, 225–236 (1991).
7. D. B. Rountree, H. F. Nijhout, *J. Insect Physiol.* **41**, 1141–1145 (1995).
8. E. V. Daniels, K. A. Mooney, R. D. Reed, *Ecol. Entomol.* **37**, 155–159 (2012).
9. C. H. Waddington, *Genet. Res.* **1**, 140–150 (1960).
10. H. F. Nijhout, *Evol. Dev.* **5**, 9–18 (2003).
11. D. B. Rountree, H. F. Nijhout, *J. Insect Physiol.* **41**, 987–992 (1995).
12. N. J. Nadeau *et al.*, *Nature* **534**, 106–110 (2016).
13. A. E. Van't Hof *et al.*, *Nature* **534**, 102–105 (2016).

Downloaded from http://science.sciencemag.org/ on November 5, 2020

14. F. Figon, J. Casas, *Biol. Rev. Camb. Philos. Soc.* **94**, 156–183 (2018).
15. I. M. Ehrenreich, D. W. Pfennig, *Ann. Bot.* **117**, 769–779 (2016).
16. J.-M. Belton *et al.*, *Methods* **58**, 268–276 (2012).
17. E. V. Daniels, R. Murad, A. Mortazavi, R. D. Reed, *Mol. Ecol.* **23**, 6123–6134 (2014).

ACKNOWLEDGMENTS

We thank B. Lazarro, A. McCune, and two anonymous reviewers for helpful comments on the manuscript, and J. Kwan, S. Molyneaux, M. Kwasnica, W. Johnsen, L. Echavez, and V. Järvi for help with butterfly husbandry. **Funding:** Supported by NSF grants IOS 1557443 and IOS 1753559 (R.D.R.). **Author contributions:** K.R.L.v.d.B. and R.D.R. conceived of and coordinated the project, acquired funding, and wrote the manuscript. K.R.L.v.d.B. and J.J.L. analyzed and curated data. K.R.L.v.d.B., J.J.L., B.J.B., R.A.F., and A.M.-V. performed experiments and collected data. **Competing interests:** The authors declare no competing interests. **Data and materials availability:** mRNA-seq and ATAC-seq data have been submitted to GEO, #GSE135523. Additional supporting material (i.e., scripts, raw datasets, etc.) are available on Dryad: https://doi.org/10.5061/dryad.rjdfn2z89.

SUPPLEMENTARY MATERIALS

science.sciencemag.org/content/370/6517/721/suppl/DC1
Materials and Methods
Tables S1 to S12
Figs. S1 to S9
References (*18*–*39*)

View/request a protocol for this paper from *Bio-protocol*.

28 August 2019; resubmitted 16 June 2020
Accepted 1 October 2020
10.1126/science.aaz3017

Downloaded from http://science.sciencemag.org/ on November 5, 2020

Science

Genomic architecture of a genetically assimilated seasonal color pattern

Karin R. L. van der Burg, James J. Lewis, Benjamin J. Brack, Richard A. Fandino, Anyi Mazo-Vargas and Robert D. Reed

Science **370** (6517), 721-725.
DOI: 10.1126/science.aaz3017

Untangling the genetics of plasticity

The common buckeye butterfly, *Junonia coenia*, exhibits plastic coloration; it has two color morphs, light tan and dark red, that depend on day length and temperature. By selecting for more and less color plasticity, van der Burg *et al.* generated butterfly lines that were used to map the genetic variants that underlie differential coloration. Genome-wide analysis and RNA sequencing identified the genes most likely to be associated with the differences in color plasticity. Inactivation of genes with CRISPR–Cas9 identified three genes that affected the red phenotype, and other techniques identified cis-regulatory, noncoding genomic variants that were correlated with coloration. From these results, the authors were able to model how genetically encoded plasticity and assimilation of the plastic trait likely evolved.

Science, this issue p. 721

ARTICLE TOOLS http://science.sciencemag.org/content/370/6517/721

SUPPLEMENTARY MATERIALS http://science.sciencemag.org/content/suppl/2020/11/04/370.6517.721.DC1

REFERENCES This article cites 37 articles, 6 of which you can access for free
http://science.sciencemag.org/content/370/6517/721#BIBL

PERMISSIONS http://www.sciencemag.org/help/reprints-and-permissions

Use of this article is subject to the Terms of Service

Science (print ISSN 0036-8075; online ISSN 1095-9203) is published by the American Association for the Advancement of Science, 1200 New York Avenue NW, Washington, DC 20005. The title *Science* is a registered trademark of AAAS.

Copyright © 2020 The Authors, some rights reserved; exclusive licensee American Association for the Advancement of Science. No claim to original U.S. Government Works

Downloaded from http://science.sciencemag.org/ on November 5, 2020

science.sciencemag.org/content/370/6517/721/suppl/DC1

Supplementary Materials for

Genomic architecture of a genetically assimilated seasonal color pattern

Karin R. L. van der Burg*, James J. Lewis, Benjamin J. Brack, Richard A. Fandino, Anyi Mazo-Vargas, Robert D. Reed*

*Corresponding author. Email: krv32@cornell.edu (K.R.L.v.d.B.); robertreed@cornell.edu (R.D.R.)

Published 6 November 2020, *Science* **370**, 721 (2020)
DOI: 10.1126/science.aaz3017

This PDF file includes:

Materials and Methods
Figs. S1 to S9
Tables S1 to S12
References

Other supplementary material for this manuscript includes:

MDAR Reproducibility Checklist (PDF)

Materials and Methods

Butterfly husbandry and selection

J. coenia adult butterflies were fed with 10% sugar water and were allowed to oviposit on *Plantago lanceolata* leaves. Larvae were fed an artificial diet as described in (*18*, *19*). For the Plastic selection line, eggs were allowed to hatch under warm conditions (27C, 16 hours of light), and larvae were either kept at these conditions or transferred to cold conditions (19C, 8 hours of light in alternating generations). Larvae from the Red line were reared continuously under warm conditions. For each generation, a minimum of 25 females and 25 males was selected. In our Plastic line, we looked for a near complete absence of red scales on the ventral side of the wings under warm conditions, and a complete coverage of red scales under cold conditions. In our Red line, we selected the butterflies with highest amount of coverage of red scales under warm conditions. Typical forewings and hindwings from both males and females are shown in fig. S1.

After we visually determined that the amount of red scale coverage per butterfly no longer changed appreciably between generations, we used photo spectrometry to measure color reflectance of butterflies from different lines and rearing conditions. Unfortunately, this method required us to sacrifice butterflies, and because we needed most animals alive to prevent inbreeding in our selection lines, we were unable to collect reflectance data for all generations. We used Ocean Optics SpectraSuite software to average 20 wavelength reflectance measurements of 200 ms each, taken with a spectrometer (Ocean Optics USB2000) equipped with a R200-7-UV/VIS reflection probe. A strobe light (PX-2 pulsed xenon light source) was used as light source. Specifically, we took measurements in the middle of the ventral hindwing near the central midline between the M3 and Cu2 veins, for 3 males and 3 females (fig. S1). We then used the mean reflectance across the spectrum (brightness) to describe wing color in a single value. We tested the difference between brightness in warm versus cold reared animals using a t-test (table S1). Because we could not measure wing color for both conditions for one genotype, we used all possible combinations of cold reared values subtracted from all warm reared values (i.e., brightness for cold reared sample 1 was subtracted from cold reared sample 1, cold reared sample 2, etc.) This gives us a distribution of reaction norm values for each line, which we used to test the differences between reaction norm distributions between the No Selection (NS) line and Red or Plastic lines (table S1).

Hormone measurements

We sampled hemolymph for the Red and Plastic lines during pupal development, at four stages, with three replicates. Sampling was done in two blocks; first, warm and cold reared pupae from the Plastic line were sampled, and then warm and cold reared pupae from the Plastic and Red line were sampled two years later. To ensure consistency between blocks, we added several safeguards and controls: (1) Sample measurement values are relative to a dilution series of known concentrations of hormone. (2) An internal standard of a known amount of synthetic hormone was used for every sample. (3) Biological replicate samples were taken both times and compared directly to each other; no difference was found (t test: $t = 0.94152$, $df = 18.21$, p-value = 0.3588), so results from both blocks were combined. (4) All measurements were done with the assistance of an experienced HPLC technician. To correct for longer development time under cold

conditions we measured time spent as pupae for both populations under both warm and cold conditions. Pupae reared under warm conditions were sampled 23.04, 46.08, 69.12, and 92.16 hours after pupation ± half an hour, representing 12%, 24%, 36% and 48% of relative development time respectively. Pupae reared under cold conditions were sampled at 51.84, 103.68, 155.52, and 207.36 hours after pupation, ± an hour, representing the same percentage of relative development time. We collected and processed hemolymph according to (*20*), with slight adaptations. In short, 20 µL of hemolymph was collected and mixed in with a 200 µL 1:1 isooctane:methanol (v/v) solution. After 20 seconds of vortexing at max speed and 20 minutes at room temperature, 15 µL of 10 ng/µL dexamethasone was added as an internal standard. Samples were spun down for 20 minutes at 20 x 10^3g at room temperature, after which the supernatant was transferred to a new microcentrifuge tube, sealed with parafilm and stored at -80°C.

Prior to hormone quantification samples were filtered for solid particles with a 45 uM pore filter (Spin-X, .22CA, VWR) before reducing the volume below 50 µL by vacuum centrifugation. Supernatant was transferred to a new vial, and methanol was added for a total volume of 60 µL. During processing, samples were kept on dry ice as much as possible. Per batch, 3 controls were processed as well: a negative control with 20 µL of PBS plus 15 µL of 10 ng/µL of internal standard, a positive control with 20 µL of PBS, internal standard, and 2.5 µL of 1ng/µL ecdysone and 20-hydroxyecdysone (20E) hormone standards (purchased from Sigma-Aldrich).

In the first block, 5 µl from each sample was analyzed in a triple-quadrupole LC-MS/MS system (Accela-Quantum Access; Thermo Scientific) equipped with a C18 reversed-phase column (Gemini NX, 3 µm, 150 x 2.00 mm; Phenomenex). The mobile phase consisted of acetonitrile (LC-MS grade; Fisher Scientific) (A) and MilliQ water (B), both containing 0.1% formic acid. The gradient program started out with 10% A which was increased to 100% in 20 min, and held at 100% for 5 min at a flow rate of 200 µL/min. Compounds were ionized in the positive electrospray mode and specific transitions were monitored (selected reaction monitoring (SRM)) for each target analyte: m/z 481.3 → 371.2 for 20E (-17 V collision energy) and 393.3 → 355.3 for dexamethasone (-11V). Argon was used as collision gas at 1.5 mTorr. To achieve absolute quantification of hormones, a dilution series with ecdysone and 20E was made ranging from 0.001 to 10 ng/µL.

In the second block, sample analysis was carried out with a Vanquish Flex UHPLC system (Dionex Softron GmbH, Germering, Germany) coupled with a TSQ Quantis mass spectrometer (Thermo Scientific, San Jose, CA). The UHPLC was equipped with a Kinetex 2.6 µm EVO C18 100 Å column (150 mm × 2.1 mm). The mobile phase consisted of (A) 1% formic acid in water and (B) 1% formic acid in acetonitrile. The temperature of the column was maintained at 30°C throughout the run and the flow rate was 500 µL/min. The elution program was the following: 0-1 min (5% B, isocratic), 1-5 min (5%-99% B, linear gradient), 5-6 min (99% B, column wash), 6-6.1 min (99%-5% B, linear gradient), 6.1-7 min (5% B, re-equilibration). The flow from the LC was directed to the mass spectrometer through a Heated Electrospray probe (H-ESI). The settings of the H-ESI were: spray voltage 4000 V, Sheath gas 50 (arbitrary unit), Auxiliary gas 20 (arbitrary unit), Sweep gas 1 (arbitrary unit), Ion transfer tube temperature 325°C, Vaporizer temperature 350°C. The mass spectrometer operating settings were the same as in phase 1. To achieve absolute quantification of hormones, a dilution series with

ecdysone and 20E was made ranging from 0.0002 to 1 ng/μL. To test for degradation, we manually determined if the 20E signal consisted of multiple components of different mass.

Cross between selection lines

To find genetic loci associated with the Red phenotype, we crossed butterflies from the Red and Plastic selection lines. To quickly score phenotypes, we created a scoring system based on (*8*). The dorsal wings were divided in three areas: (a) forewing tip, (b) proximal and median region of the hindwing (c) distal region of the hindwing (Fig S2A). For each region, a score of 1-5 was assigned: (1) 0% red scales, (2) 0-25% red scales, (3) 25-50% red scales, (4) 50-75% red scales, (5) 75-100% red scales. Percentage values were approximated by eye using a color scale as comparison (shown in fig. S2B-D). In fig. S3, the mean value of these scores is shown. Adult butterflies were called as heterozygous if their wing color score fell between the selection line color scores (fig. S3A, B).

Since female butterflies have reduced or absent recombination (*21*), we created F3 crosses as shown in fig. S3C. First, we generated heterozygous crosses from a Red male with a Plastic female (fig. S3D). A heterozygous male from this cross (fig. S3D) was then crossed with a homozygous female from the Red line—approximating a backcross—creating an F2 generation of mostly heterozygotes and homozygotes Red butterflies (fig. S3E). Heterozygous-like males and females from this line were crossed in four pairs, generating of a wide range of phenotypes (fig. S3F). From the two largest families, the 20 most pale and 21 most red (i.e., presumptive homozygous Plastic and homozygous Red) were selected for sequencing (table S2)

Genotyping, variant calling, and genome wide association

Genomic DNA was extracted from selected butterflies using the Qiagen DNeasy extraction kit (Qiagen, 69506). Libraries were prepared using the Nextera kit (Illumina #15028212), with half reactions. In addition to 41 F3 individuals, we sequenced F2, F1 and F0 on a NextSeq 500 to between 2x and 5x read depth as paired end 2 x 150 length reads (for a full list, see table S3). Reads were trimmed and adapters were removed using cutadapt (*22*) to a minimum quality score of 30, and a minimum length of 10. Sequencing reads were aligned to the *J. coenia* reference genome (*23*) with bowtie2 (*24*). We used the GATK HaplotypeCaller followed by GenotypeGVCFs to call variants (*25*). Variants were filtered using the metrics shown in table S4. After filtering, 497,608 variants were left.

We used PLINK software v1.9 (*26*) for our association test. As our variable phenotype, we used the average score of the amount of red in three regions of the wings as described previously (fig. S2). We used the first three principal components (plink --pca) as covariates to account for family structure. This resulted in the lowest genomic inflation (lambda of 1.07). See fig. S4A-B for segregation along pca axes. We also used sex as a covariate, as females tend to be darker than males. Thus, we ran Plink with the following parameters: --assoc --covar plink.eigenvec --covar-name PC1, PC2, PC3 --linear sex --adjust --allow-extra-chr. For the qqplot, see fig. S4C. We used the unadjusted *p* values <1e-5 for downstream analyses. We used snpeff to determine variant

functionality. For a list of all single nucleotide polymorphisms with a p-value <1e-05 and their functionality, see table S5.

mRNA-seq and ATAC-seq library preparation

mRNA-seq and ATAC-seq library preparation followed previously described protocols (*23*, *27*, *28*). In short, we collected three replicates of hindwing tissue at four developmental stages: wandering stage of a 5th (last) instar caterpillar (5th), prepupae (pp), 72 hours after pupation (72h), and six days after pupation, when ommochrome pigments appear (d7) (fig. S5A). We sampled both left and right wings, and randomly chose one wing for immediate use in the ATAC-seq assay, and stored the opposing wing in Trizol for later RNA extraction. For ATAC-seq, nuclei were extracted and processed as previously described (*29*). For RNA extraction, we used the PureLink RNA PLUS protocol (Invitrogen, 12183018A) to extract RNA. To make sequencing libraries, we used the Ultra RNA Library Prep Kit (NEBNext, E7530). We sequenced all ATAC-seq and mRNA-seq libraries at the Cornell Genomics Facility, using 2 x 36 bp reads from an Illumina NextSeq 500. For ATAC-seq, we obtained a minimum of 10 million aligned reads after removal of duplicate and non-uniquely aligning read (table S6). For RNA-seq, we obtained a minimum of 20 million aligned reads (table S7). Although the mRNA-seq and ATAC-seq data from the Plastic line were published previously (*23*), data from both Plastic and Red lines were collected simultaneously.

mRNA-seq and ATAC-seq data analysis

We aligned our mRNA sequencing reads to the *J. coenia* reference genome (v1.0) and used the transcriptome (v1.0) to count reads within genes for each individual. Differential gene expression was analyzed with DeSEQ2 (*30*). Genes showing a change in expression levels between lines were deemed significant when the adjusted p value < 0.05 (Wald test, DeSEQ2 default settings). Clustering analysis revealed that different stages and lines largely clustered together (fig. S5B, C).

ATAC-seq reads were also aligned to the *J. coenia* reference genome, and duplicate and multiple aligning reads were removed from further analysis. We assessed read depth Pearson correlations between replicates within bins of 1 kB using the Deeptools software package (*31*) (fig. S6A). When correlations higher than 90% between replicates were verified, we merged replicate samples together, and called peaks on each assay per developmental stage using fseq with parameters -l 600 (*32*), after which the separate call sets were merged together. This was done to ensure small peaks only occurring in one developmental stage in one line would still be included in the analysis. Thus, we ended up with a total set of 171,888 peaks. To assess data quality, we determined enrichment of reads at transcription start sites (fig. S6B), as well as FRiP (Fragment of Reads in Peaks) and PBC (PCR Bottlenecking Coefficient) scores (table S6). For a screenshot of example ATAC-seq data tracks see fig. S6C. Next, we used DeSEQ2 to do pairwise comparisons between Red and Plastic per developmental stage. Of the 171,888 peaks, 580 (.34%) were significantly different between Red and Plastic lines at stage 5th, 2,385 (1.34%) were different at stage pp, 1,449 (0.84%) were different at stage 72h, and 18,862 (11.0%) were different at stage d7. From this, we infer that the regulatory landscape between the two lines is most different late in development, when pigments, include red ommochromes, are being produced. In the non-coding region surrounding *cortex* (within

50 kB of the transcription start site, TSS), the regulatory landscape was remarkably similar between the lines, with no significant differences in magnitude of accessibility. For *trehalase* we found three nearby regions showing significant accessibility differences between lines. Lastly, CRE activity was substantially different in the non-coding region near *herfst* throughout development, with five ATAC-seq peaks showing significant accessibility differences.

Hi-C data analysis

To test which *cis*-regulatory elements (CREs) could be driving changes in gene expression, we used Hi-C, a chromatin confirmation capture technique. This assay allows us to investigate which loci in are physically interacting above expected levels with other loci anywhere in the genome (*16*, *33*). In other words, we can show that CREs are physically linked to transcription start sites of genes, which is direct evidence of regulatory activity of that CRE on a specific gene (*28*, *34*).

For Hi-C library prep, we collected 26 5th instar wings, and 26 72h wings. Hi-C libraries were prepared following the *in situ* Hi-C protocol (*33*) with minor modifications (*28*). Hi-C sequencing reads were processed with Juicer (*35*), using the *J. coenia* reference genome (v1.0). To visualize 3D interactions, we made virtual circular chromosome conformation capture (4C) plots using a previously published custom script (*34*). Significantly enriched distal CRE-to-promotor interactions were determined with a Fisher's exact test of expected and observed read counts as previously described (*34*, *36*). We tested whether loop interactions of CREs with promotors (putative Transcription Start Sites) of our three genes were significant. For *cortex*, we found no differences in ATAC-seq peaks between Red and Plastic lines. However, we tested 9 peaks within 10 kB of a significant nucleotide variant, and found 7 peaks that showed an interaction with the *cortex* promotor, at the fifth instar developmental stage when *cortex* is differentially expressed (table S9, fig. S7). The *cortex* promotor site was confirmed and reannotated using the *Heliconius melpomene melpomene* genome assembly 2.5 (*20*, lepbase.org). For *trehalase*, we tested loop-interactions for four ATAC-seq peaks: One near a SNP of interest (treh_ATAC-peak-1), and three others that were differentially accessible between the selection lines. One peak (treh_ATAC-peak-2) indeed showed a significant loop interaction the *trehalase* promotor, at 72 hours after pupation (fig. S7 and table S9). For *herfst*, we tested five ATAC-seq peaks that were significantly different at both developmental stages. At 5th instar, we found two ATAC-seq peaks that showed a loop interaction, and at 72 hours after pupation we found 3 peaks. Interestingly, these peaks were located at promotor sites of nearby genes. These three peaks also showed three-way interactions (Fig. 3), suggesting a hub where multiple regulatory elements form a tight network (fig. S7 and table S9).

CRISPR/Cas9 genome editing

We produced G0 somatic mosaic deletion knockouts using the technique described in (*38*). In short, we designed two pairs of single guide RNAs (sgRNAs) for each candidate gene (table S10). We targeted areas surrounding protein domains to make large deletions (fig. S8A). sgRNAs were synthesized by Synthego. Pairs of sgRNAs were mixed with Cas9 protein (IDT, #196814127). We then injected the sgRNA/Cas9 mixture into developing embryos within .5 to 2.5 hours after oviposition, at various

concentrations (table S11). To confirm mutations, we extracted DNA from bodies of clonal mutants and PCR amplified the products. If clear, multiple bands were seen with gel electrophoresis, the shorter band was cut out and sequenced using Sanger sequencing. If the smaller band was at too low of a concentration, the larger band was gel purified, sequenced and analyzed with TIDE – a software package that determines the mutation frequency from CRISPR/Cas9 induced mutations (*39*) (fig. S8B). Thus, we have sequence confirmation of mutations for all sgRNAs except for one out of four *trehalase* sgRNAs, due to a nucleotide variant in the guide sequence of sgRNA2.

For three genes, *cortex, trehalase,* and *herfst*, we observed several mutant phenotypes (fig. S9 and table S12). For *herfst* we saw reduction and/or loss of dorsal eyespots (fig. S9A), wing size distortion (fig. S9B), pigment reduction (fig. S9C), and red scales turning tan (fig. S9D). For *trehalase*, we also observed missing eyespots (fig. S9E), size distortion (fig. S8F), missing pigments (fig. S9G), and red scales turning tan (fig. S9H). For c*ortex*, we observed black dorsal eyespot centers turning iridescent, and other black dorsal patterns disappearing completely (fig. S9I), and red scales turning tan (fig. S9J). No mutant phenotypes were observed in our *Dscam3* experiments, although we cannot rule out that successful knockouts may have been embryonic lethal.

Fig. S1. Representative phenotypes from selection lines.
Males and females reared under cold and warm conditions before and after selection are shown. The ellipse in the top left marks where spectrometer measurements were taken.

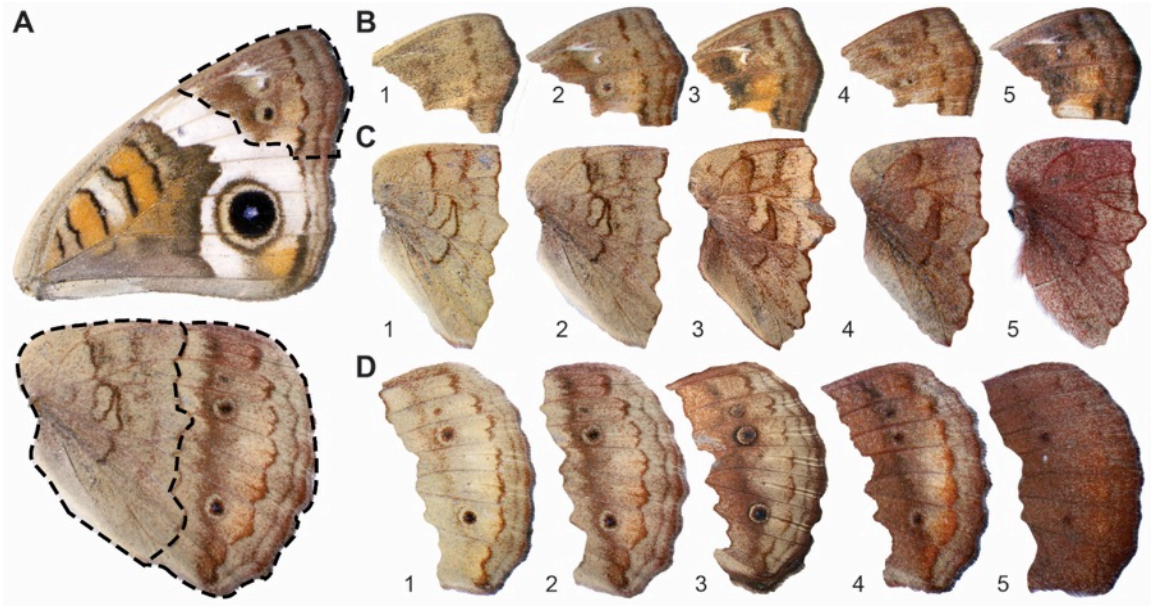

Fig. S2. Color scale used for scoring mapping phenotypes.

(A) Different parts of the wings were scored separately. (B-D) For each region, a score of 1-5 was assigned: (1) 0% red scales, (2) 0-25% red scales, (3) 25-50% red scales, (4) 50-75% red scales, (5) 75-100% red scales. Percentages were determined by visual observation.

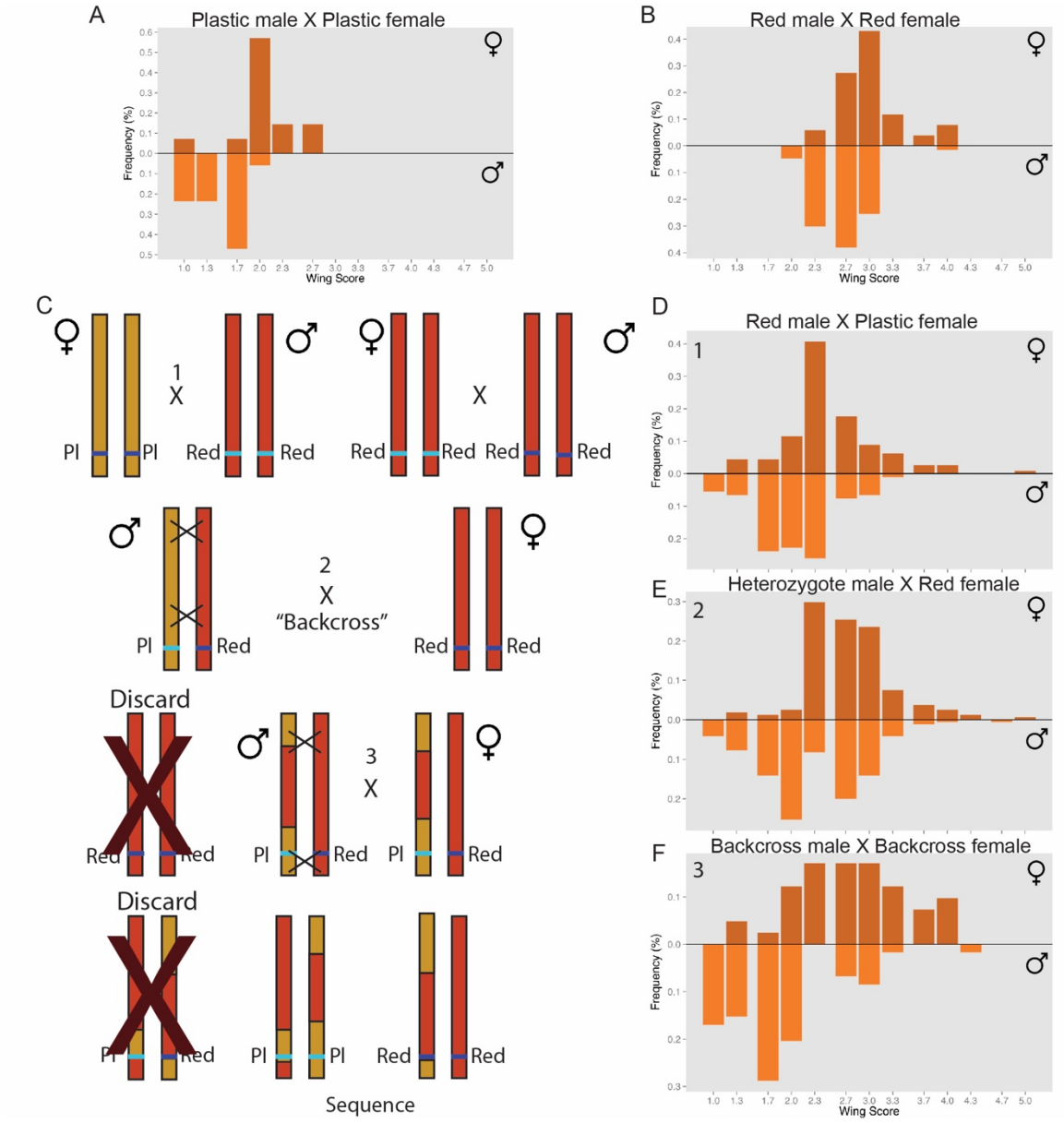

Fig. S3. F3 cross between butterflies from the Red and Plastic lines.

(A) Distribution of phenotypes of the offspring of a Plastic male and female. Scores are the average values of the three scores described in fig. S2. Female phenotypes, which tend to be darker on average, are summarized in the top histogram, while males phenotypes are illustrated in the bottom histogram. (B) Distribution of phenotypes of the offspring of a Red male and female. (C) Cross schedule between the lines. (D-F). Phenotype distributions of the F1 (D), F2 (E), and F3 (F) crosses. The most extreme phenotypes from the F3 cross were sequenced.

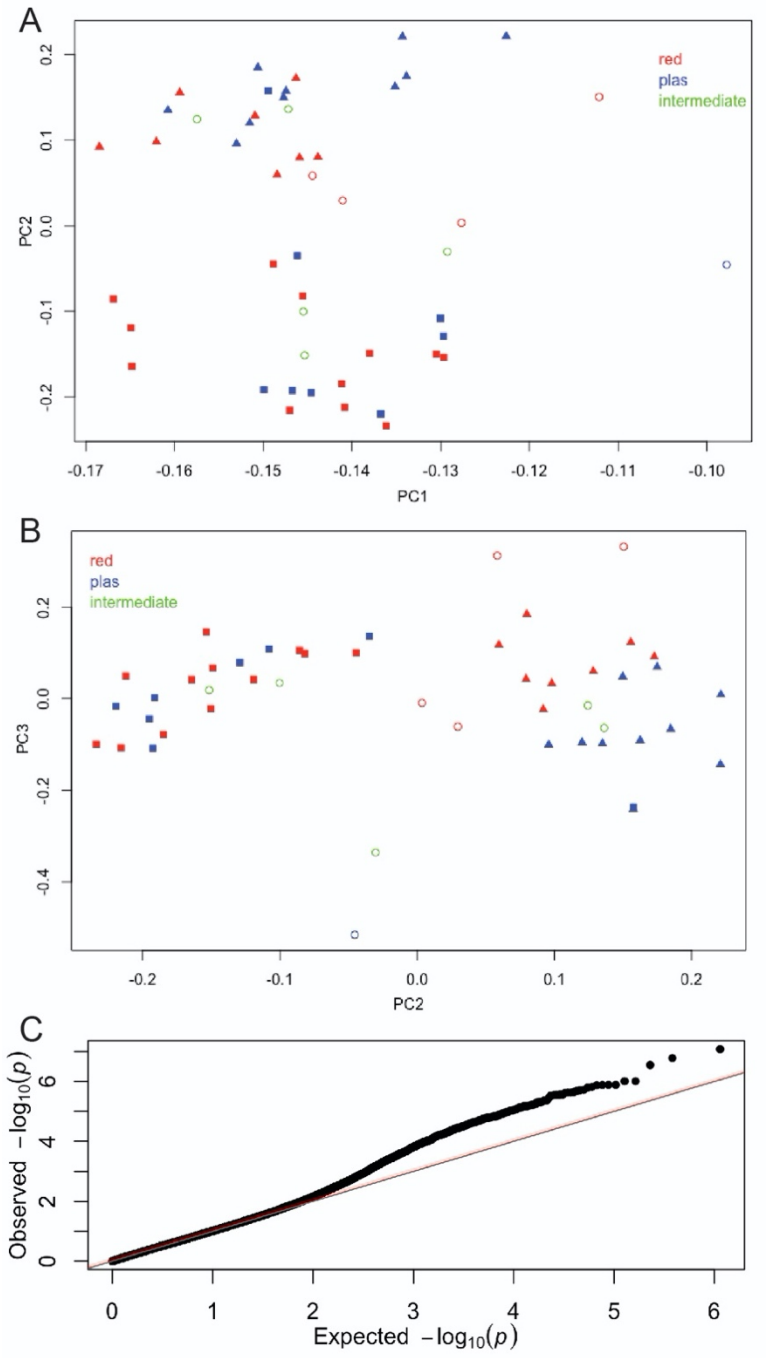

Fig. S4. Principal components and genomic inflation plot.

(A-B) The first three principal components were used as covariates in the genome wide association analysis to account for family structure. Colors indicate phenotype. Squares and triangles indicate the F3 offspring from two different families, and open circle indicate parental genotypes. (C) Genomic inflation test (lambda of 1.07).

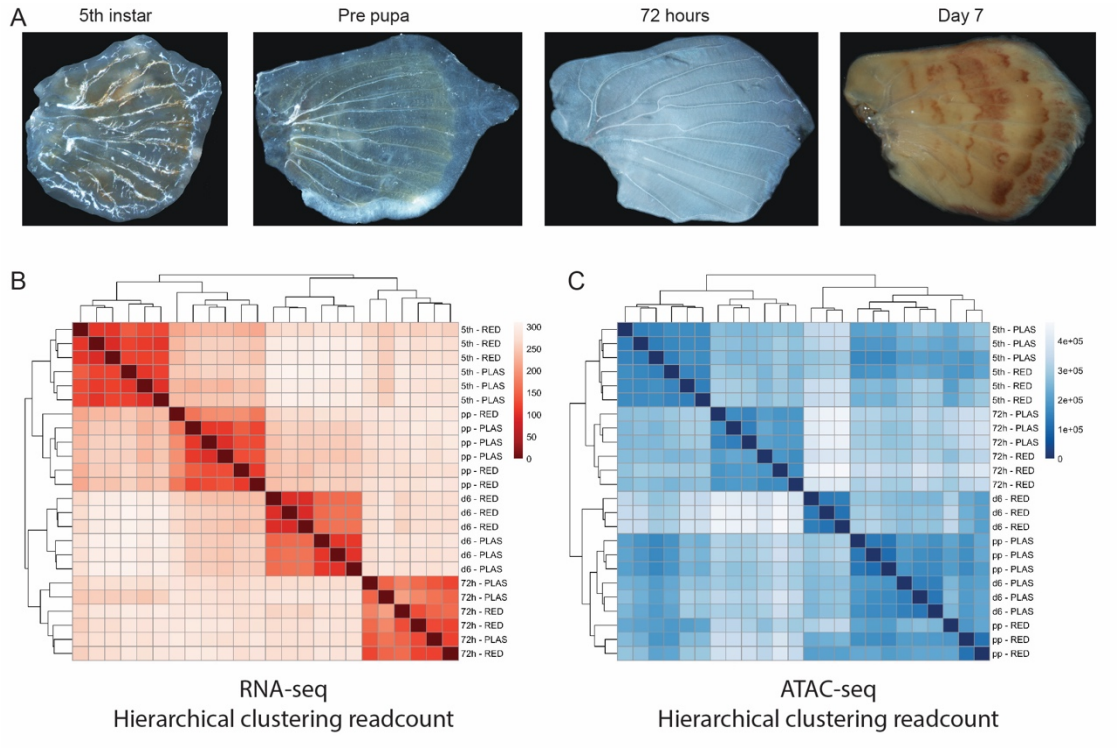

Fig. S5. ATAC-seq and RNA-seq sampling and clustering.

(A) Samples were taken at four different developmental stages, as described above. (B) RNA-seq data cluster by stage and selection line. (C) ATAC-seq data cluster by stage and selection line.

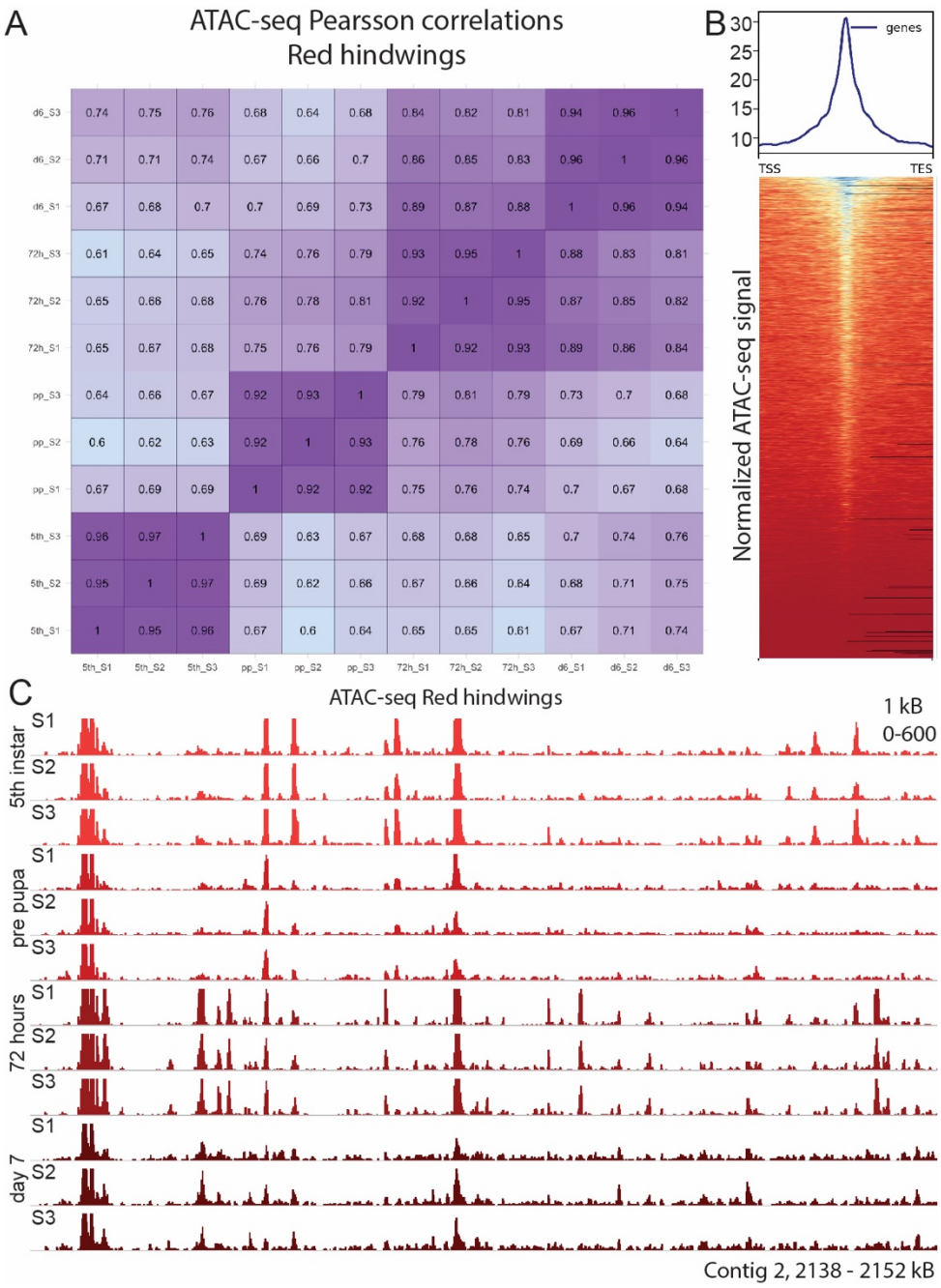

Fig. S6. ATAC-seq quality metrics.

(A) Pearson correlation between ATAC-seq libraries shows that replicates are highly correlated. (B) ATAC-seq reads are enriched at promoters (i.e., transcription start sites), as would be predicted. (C) Screenshot of example ATAC-seq data tracks across all replicates (S1-S3) and developmental stages.

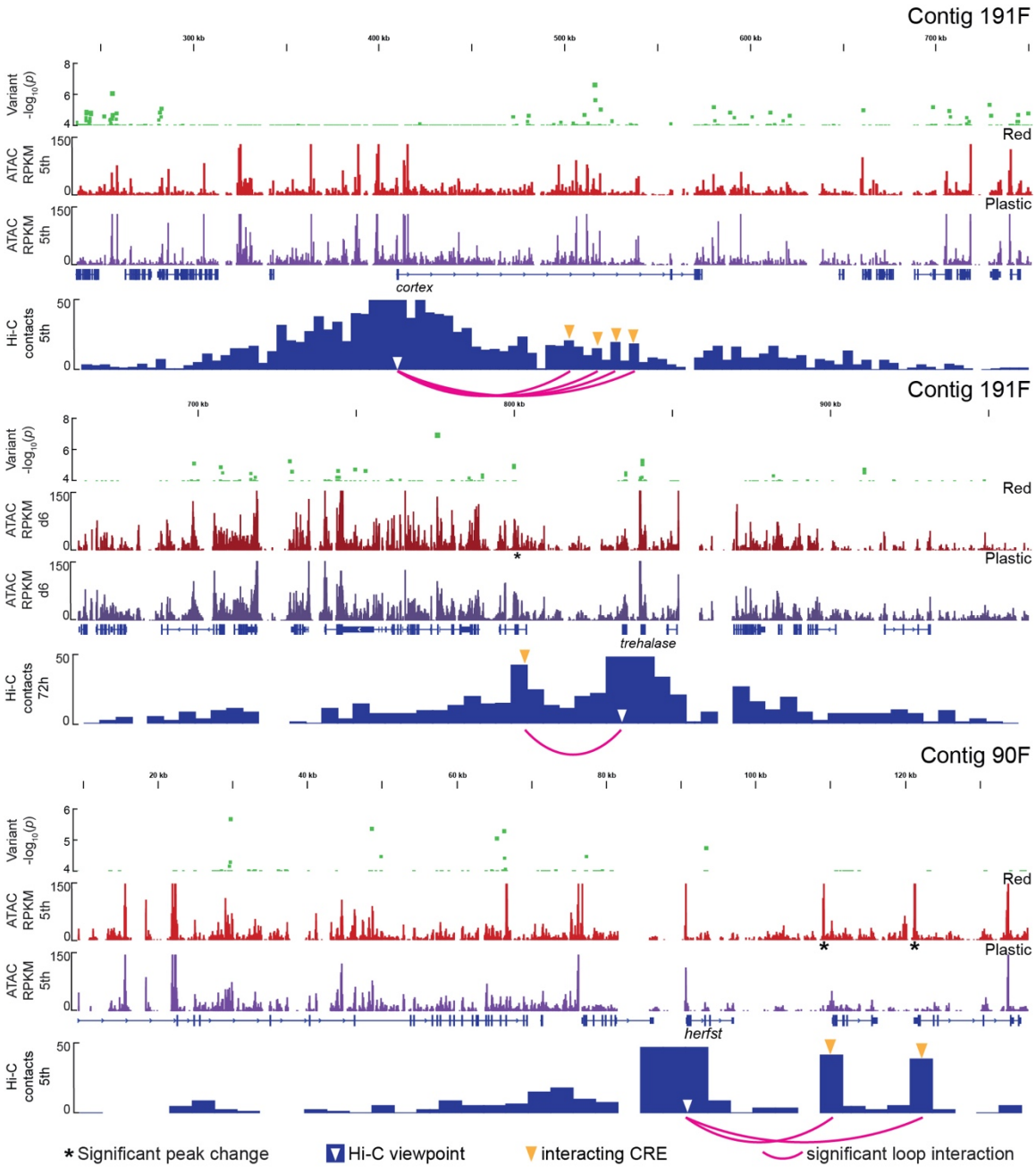

Fig. S7. Broad-scale overview of Hi-C loop interactions.

Nucleotide associations (top, green) and ATAC-seq tracks (middle, red and purple) are shown. For the Hi-C contact data (bottom, blue), promotor sites are used as viewpoints (white triangles). Yellow arrows and pink lines mark ATAC-seq peaks we tested for significant physical interactions. Asteriks mark variable accessible peaks interacting with a causal gene. Note that Fig. 3, in the main text, displays a complementary analysis using presumptive CREs as viewpoints.

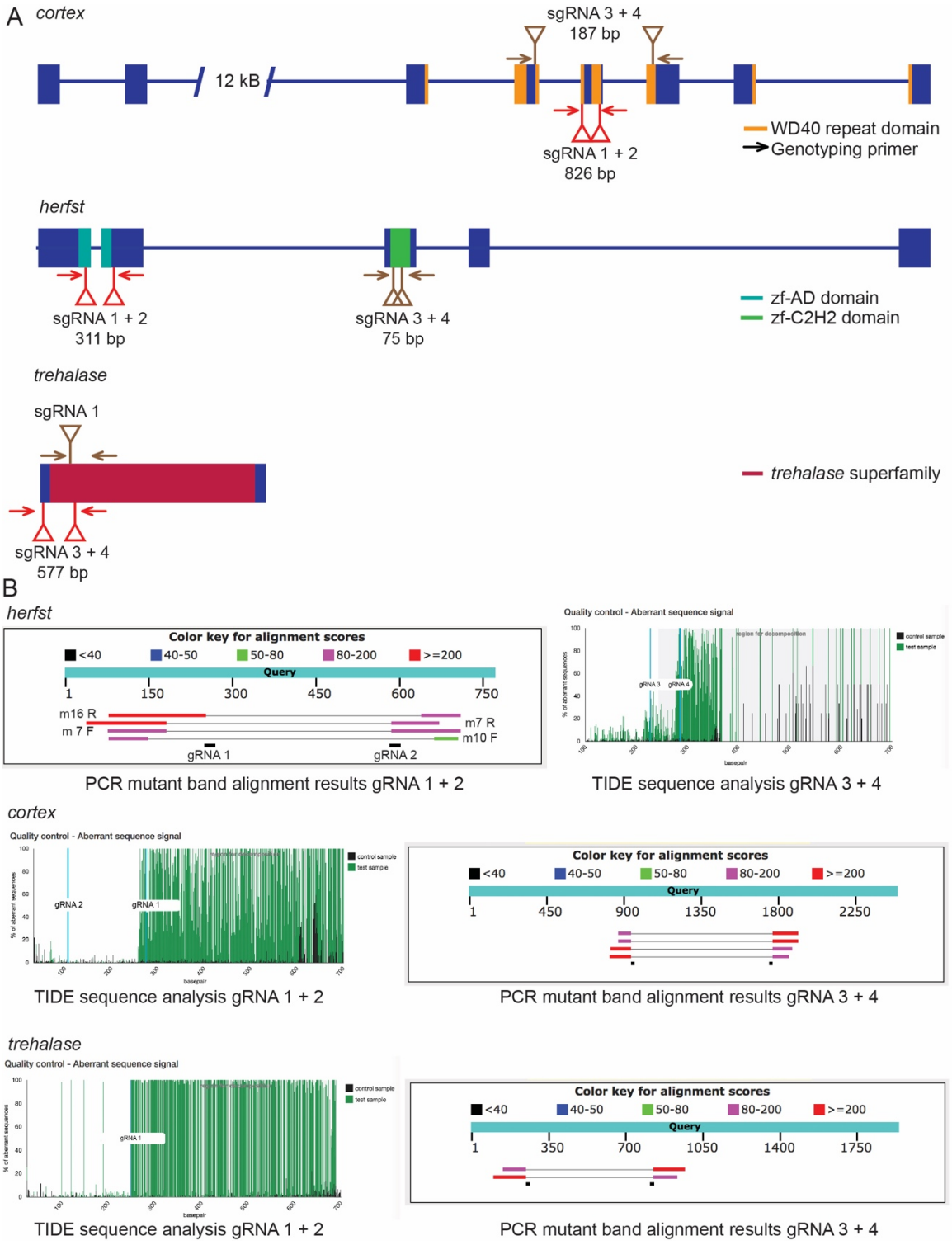

Fig. S8. CRISPR/Cas9 sgRNA design and genotyping.

(A) Location of the different sgRNAs in respect to the protein domains. (B) Genotyping results using either PCR product Sanger sequencing and BLAST, or TIDE.

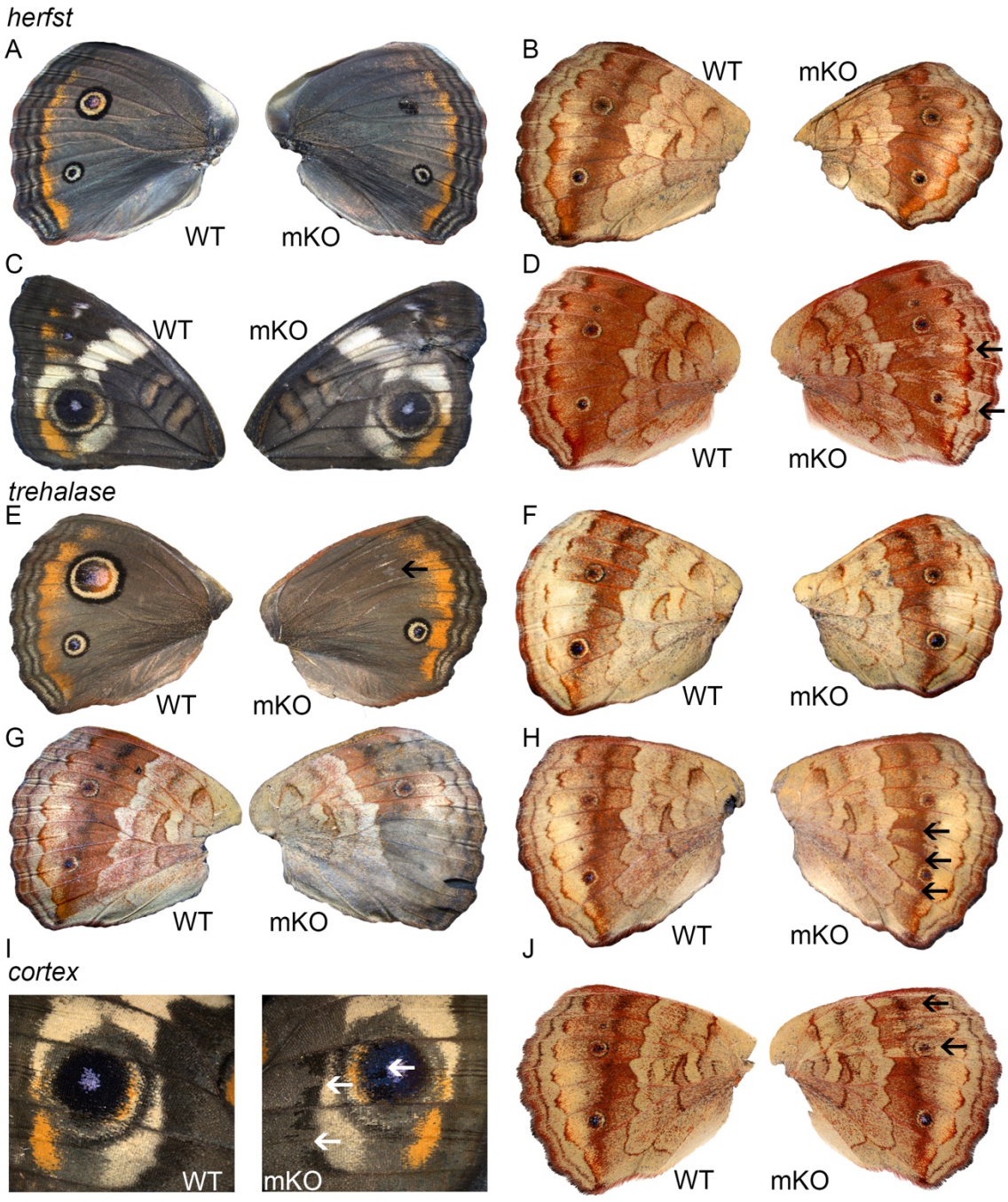

Fig S9. Representative CRISPR/Cas9 mutants for common phenotypes.

(A-D) Mutants from knocking out *herfst*. (E-H) Mutants for knocking out *trehalase*, I-J, mutants for knocking out *cortex*. Common mutants were smaller eyespots (A and E), wing size distortion (B and F), reduced pigmentation (C and G) and red pigments turning tan (D, F and J). Unique to *cortex*, we saw the center eyespot become more iridescent while losing melanic coloration (I).

Table S1. Wing color and reaction norm comparisons.

Spectrometer reflectance data collected for hindwings. Warm and cold reared butterfly wing color is compared (top), and reaction norms of the Red and Plastic selection lines are compared to the No Selection line (NS) (bottom). A t test was used for all comparisons.

	N	mean (warm) wing color	SD (warm) wing color	mean (cold) wing color	SD (cold) wing color	t	df	p
NS	14	19.53	±2.45	14.17	±3.14	3.46	9.23	**0.0069**
Plastic	12	25.65	±3.23	11.28	±.44	10.79	5.19	**<0.0001**
Red	16	17.74	±2.12	14.77	±3.61	2.07	14.00	0.057

	N	Mean reaction norm	SE reaction norm	t	df	p
NS	14	5.36	±.54	NA	NA	NA
Plastic	12	14.37	±.50	-12.26	81.41	**<0.0001**
Red	16	2.97	±.51	-3.22	103.39	**0.0017**

Table S2. Phenotype information for individuals used for whole genome resequencing.

Cross	ID	Sex	Generation	fw	hwmed	hwdist	mean
B46	BC46F	female	F1	3	2	3	2.67
B46	BC46F10	female	F2	3	2	2	2.33
B46	BC46F8	female	F2	3	2	3	2.67
B46	BC46M	male	F1	2	1	2	1.67
B46	BC46M11	male	F2	3	2	3	2.67
B46	BC46M9	male	F2	4	2	3	3.00
C20	CR20F	female	P	4	2	3	3.00
C20	CR20M	male	P	4	1	2	2.33
C29	CR29F	female	P	4	2	3	3.00
C29	CR29M	male	P	1	1	1	1.00
f218	F218_F2	female	F3	3	2	2	2.33
f218	F218_F1	female	F3	4	2	3	3.00
f218	F218_F6	female	F3	3	3	3	3.00
f218	F218_F4	female	F3	4	3	3	3.33
f218	F218_F8	female	F3	5	2	3	3.33
f218	F218_F7	female	F3	5	3	4	4.00
f218	F218_M9	male	F3	1	1	1	1.00
f218	F218_M17	male	F3	2	1	2	1.67
f218	F218_M20	male	F3	2	1	2	1.67
f218	F218_M23	male	F3	2	1	2	1.67
f218	F218_M3	male	F3	2	1	2	1.67
f218	F218_M5	male	F3	2	1	2	1.67
f218	F218_M6	male	F3	2	1	2	1.67
f218	F218_M14	male	F3	3	2	3	2.67
f218	F218_M15	male	F3	3	2	3	2.67
f218	F218_M7	male	F3	3	2	3	2.67
f218	F218_M1	male	F3	4	2	3	3.00
f218	F218_M10	male	F3	4	2	3	3.00
f218	F218_M11	male	F3	4	2	3	3.00
f218	F218_M21	male	F3	4	2	3	3.00
f218	F218_M22	male	F3	5	4	4	4.33
f220	F220_F12	female	F3	2	1	1	1.33
f220	F220_F8	female	F3	2	2	1	1.67
f220	F220_F13	female	F3	3	2	2	2.33
f220	F220_F5	female	F3	3	2	2	2.33

f220	F220_F6	female	F3	3	2	2	2.33
f220	F220_F16	female	F3	3	3	3	3.00
f220	F220_F11	female	F3	4	3	3	3.33
f220	F220_F4	female	F3	5	3	3	3.67
f220	F220_F9	female	F3	5	3	3	3.67
f220	F220_F14	female	F3	5	3	4	4.00
f220	F220_F3	female	F3	3	5	4	4.00
f220	F220_M1	male	F3	1	1	1	1.00
f220	F220_M16	male	F3	1	1	1	1.00
f220	F220_M20	male	F3	1	1	1	1.00
f220	F220_M7	male	F3	1	1	1	1.00
f220	F220_M9	male	F3	1	1	1	1.00
f220	F220_M12	male	F3	2	1	1	1.33
f220	F220_M11	male	F3	4	2	3	3.00
f220	F220_M22	male	F3	5	2	3	3.33

Table S3. Summary of whole genome resequencing data.

ind_ID	Sequencing Depth (Coverage)	Breadth at 1X (% Genome covered)	Total number of raw reads (M)	Total number of postQC reads (M)	% reads mapped
BC46F	3.26638	0.752526787	15479148	14804604	76.69%
BC46F10	3.50684	0.842437717	14734736	14125288	94.69%
BC46F8	5.94941	0.558397565	22466868	16476781	98.76%
BC46M	4.49945	0.830180079	18911742	18183942	94.47%
BC46M11	3.92014	0.78975386	16038344	15067140	95.28%
BC46M9	3.4174	0.721849329	13594798	12840392	94.46%
CR20F	2.94501	0.638817772	13020174	12278258	77.46%
CR20M	4.11675	0.62527162	15593280	14754232	88.75%
CR29F	3.70564	0.601337169	18732460	17681068	65.03%
CR29M	2.23883	0.513554987	10947652	10302454	54.70%
F218_F1	5.02451	0.70652585	18525214	17646096	94.65%
F218_F2	5.66881	0.863607748	28891028	27523014	95.15%
F218_F4	3.41506	0.741909044	14216366	13411258	94.13%
F218_F6	7.38827	0.780561127	34268796	33039682	95.02%
F218_F7	5.5778	0.848679857	24802400	23739346	94.54%
F218_F8	3.53733	0.82265374	53457068	52654670	95.10%
F218_M1	5.78796	0.831842456	26589430	25613274	95.03%
F218_M10	3.09536	0.701707021	12103794	11401816	94.73%
F218_M11	3.75708	0.7505338	15877126	15031910	95.17%
F218_M14	7.39616	0.83585421	36896382	35589834	95.21%
F218_M15	7.17629	0.90384481	170859040	117937650	94.87%
F218_M17	3.88542	0.816234803	17078882	16120728	94.21%
F218_M20	4.95455	0.83072066	21721334	20822754	95.15%
F218_M21	4.9478	0.81920998	21983336	21060686	94.39%
F218_M22	7.00949	0.897957348	33999332	32792634	94.97%
F218_M23	8.83534	0.87134516	41319952	39811488	95.12%
F218_M3	6.83369	0.847319523	34286348	33126118	94.68%
F218_M5	5.32529	0.684405781	19303038	18458408	94.90%
F218_M6	5.89535	0.864075834	27534224	26425546	94.70%
F218_M7	2.80209	0.713374424	10554250	9971064	94.60%
F218_M9	3.87345	0.719583345	15145422	14470592	94.68%
F220_F11	3.20014	0.787380024	12919716	12315210	94.85%
F220_F12	4.70042	0.83066899	19940062	19048468	94.84%
F220_F13	5.61004	0.831157262	25440006	24441806	95.03%

F220_F14	7.39521	0.81043637	34415166	33128626	95.34%
F220_F16	2.55489	0.643945722	8770064	8320458	94.32%
F220_F3	2.51387	0.681707221	9145428	8636904	93.81%
F220_F4	4.96955	0.847395168	21941290	20994228	96.21%
F220_F5	4.43692	0.83335294	18341420	17517444	95.43%
F220_F6	4.56969	0.864641007	19829688	18995298	94.85%
F220_F8	5.17953	0.780659035	23088716	21978550	94.99%
F220_F9	5.19962	0.852211859	22006646	21141450	95.47%
F220_M1	5.77241	0.822812631	24899018	23856192	95.65%
F220_M11	2.84352	0.651970338	11211282	10141858	95.56%
F220_M12	1.9105	0.039959978	471310	450682	93.90%
F220_M16	4.09729	0.767521941	17040244	16317508	94.98%
F220_M20	5.45776	0.829492926	25036728	24063788	95.19%
F220_M22	5.70122	0.86679296	26260392	25210096	94.90%
F220_M7	4.61052	0.791122099	19625106	18772220	95.69%
F220_M9	6.40632	0.879476682	31347130	30115516	95.55%

Table S4. Nucleotide variant calling filters.

Filter	Value
Standard emit confidence	>30
Allele count	<3
Overall depth	<500
Quality by depth	<3.0
Strand bias (FS)	>60
MQ (Mapping quality)	<20
MQRankSum (Mapping quality variant vs ref)	<-12.5
ReadPosRankSum (bias within read)	<-8
Genotype depth	<3 >75
Missing data	>15 individuals

Table S5. Nucleotide variant annotations.

Putative effects of variants as determined by SNPeff.

SNP location	A0	A1	Non missing	BETA	STAT	P	Annotation
000010F-3224267	G	T	38	-0.6719	-5.291	8.53E-06	intergenic_region
000044F-1114419	A	T	38	-0.6324	-5.25	9.59E-06	intergenic_region
000044F-1350084	C	T	38	-0.764	-5.249	9.64E-06	downstream_gene_variant
000044F-1350087	A	G	38	-0.764	-5.249	9.64E-06	downstream_gene_variant
000044F-1997315	A	G	40	-0.7735	-5.861	1.31E-06	upstream_gene_variant
000044F-1997330	G	T	40	-0.7735	-5.861	1.31E-06	upstream_gene_variant
000044F-2117325	C	T	38	-0.8373	-5.265	9.18E-06	intergenic_region
000044F-2137552	T	C	39	-0.6094	-5.357	6.43E-06	upstream_gene_variant
000044F-2166198	C	T	39	-0.7201	-5.632	2.86E-06	downstream_gene_variant
000044F-2205700	G	A	41	-0.8212	-6.51	1.65E-07	upstream_gene_variant
000044F-2205750	T	C	41	-0.791	-5.774	1.53E-06	upstream_gene_variant
000044F-2205771	G	C	40	-0.7951	-5.732	1.92E-06	upstream_gene_variant
000044F-2214385	T	C	42	-0.8226	-5.472	3.53E-06	downstream_gene_variant
000044F-2269613	C	G	37	-0.8873	-5.689	2.98E-06	intron_variant
000044F-2269704	G	A	41	-0.8019	-5.385	5.00E-06	intron_variant
000044F-2279207	A	G	38	-0.7515	-5.277	8.87E-06	intron_variant
000044F-2286155	G	A	39	-0.8605	-5.315	7.28E-06	intron_variant
000044F-2294176	T	C	39	-0.8844	-5.756	1.98E-06	intergenic_region
000044F-2400970	C	T	38	-0.7518	-5.373	6.71E-06	synonymous_variant
000044F-2456218	G	T	39	-0.7738	-5.46	4.74E-06	intergenic_region
000044F-2467786	C	T	39	-0.7824	-5.343	6.70E-06	intergenic_region
000044F-2467812	T	A	39	-0.7824	-5.343	6.70E-06	intergenic_region
000090F-29734	A	T	39	-0.6766	-5.69	2.40E-06	intron_variant
000090F-48681	C	A	39	-0.8296	-5.445	4.97E-06	downstream_gene_variant
000090F-65386	A	C	39	-0.7508	-5.215	9.79E-06	intron_variant
000090F-66350	A	C	40	-0.7803	-5.368	5.71E-06	upstream_gene_variant
000090F-1775714	G	A	39	-0.9213	-5.491	4.33E-06	intergenic_region
000152F-256219	A	G	40	-0.7466	-5.291	7.19E-06	intergenic_region
000152F-375441	A	G	39	-0.6878	-5.303	7.54E-06	missense_variant
000152F-591483	A	C	39	-0.79	-5.378	6.05E-06	synonymous_variant
000152F-591488	G	A	40	-0.8299	-5.601	2.84E-06	synonymous_variant
000152F-591497	A	T	40	-0.8299	-5.601	2.84E-06	synonymous_variant
000152F-605065	C	G	41	-0.8643	-5.822	1.32E-06	synonymous_variant
000152F-682188	A	G	41	-0.7049	-5.756	1.62E-06	intergenic_region

000152F-726286	A	G	41	-0.7642	-5.323	6.03E-06	downstream_gene_variant
000152F-752431	G	A	40	-0.8159	-5.26	7.90E-06	upstream_gene_variant
000152F-838606	C	T	38	-0.8086	-5.335	7.50E-06	synonymous_variant
000152F-955722	A	T	38	-1.059	-5.926	1.35E-06	downstream_gene_variant
000152F-1014568	T	C	41	-0.7996	-5.311	6.25E-06	upstream_gene_variant
000152F-1176345	C	A	43	-0.8995	-5.617	2.07E-06	intergenic_region
000191F-134421	T	A	41	-0.6024	-5.222	8.20E-06	upstream_gene_variant
000191F-134430	T	AGA	41	-0.6132	-5.39	4.93E-06	upstream_gene_variant
000191F-134499	T	C	38	-0.6935	-5.519	4.39E-06	upstream_gene_variant
000191F-169431	G	A	41	-0.7426	-5.557	2.96E-06	synonymous_variant
000191F-169434	G	A	42	-0.7349	-5.612	2.29E-06	synonymous_variant
000191F-187601	G	A	40	-0.8276	-5.329	6.42E-06	5_prime_UTR_variant
000191F-211036	T	G	39	-0.7405	-5.643	2.76E-06	intron_variant
000191F-211050	A	C	39	-0.7405	-5.643	2.76E-06	intron_variant
000191F-230965	TA	-	39	-0.7712	-5.395	5.74E-06	3_prime_UTR_variant
000191F-256823	AG	-	38	-0.954	-6.035	9.80E-07	intergenic_region
000191F-256824	T	C	38	-0.954	-6.035	9.80E-07	intergenic_region
000191F-283154	G	T	37	-0.8277	-5.315	8.70E-06	upstream_gene_variant
000191F-516619	A	T	42	-0.8425	-6.296	2.80E-07	intergenic_region
000191F-516674	G	T	39	-0.7475	-5.696	2.36E-06	intergenic_region
000191F-516680	C	A	39	-0.7475	-5.696	2.36E-06	intergenic_region
000191F-519760	T	A	41	-0.6695	-5.182	9.24E-06	intergenic_region
000191F-580457	A	T	38	-0.856	-5.37	6.76E-06	intergenic_region
000191F-698783	A	G	40	-0.7359	-5.314	6.72E-06	intron_variant
000191F-729185	C	T	40	-0.7127	-5.42	4.89E-06	downstream_gene_variant
000191F-775758	G	T	38	-0.9857	-6.901	8.22E-08	synonymous_variant
000191F-800044	G	A	40	-0.8912	-5.215	9.05E-06	upstream_gene_variant
000191F-800045	C	A	40	-0.8912	-5.215	9.05E-06	upstream_gene_variant
000191F-840646	G	A	41	-0.7895	-5.255	7.40E-06	missense_variant
000191F-840697	C	T	40	-0.8143	-5.466	4.26E-06	synonymous_variant

Table S6. ATAC-seq library information and quality scores

FRiP = Fragments of Reads in Peaks, PBC = PCR Bottlenecking Coefficient

Library name	Aligned reads	FRiP	PBC
RED_5th_HW_S1	11845051	0.3229836	0.8971168
RED_5th_HW_S2	9709799	0.3003413	0.9229028
RED_5th_HW_S3	12657117	0.346335	0.8768509
RED_pp_HW_S1	16312566	0.3426338	0.9130481
RED_pp_HW_S2	16570104	0.3365143	0.913818
RED_pp_HW_S3	10057382	0.3377661	0.9369409
RED_72h_HW_S1	10374815	0.3608055	0.8671147
RED_72h_HW_S2	12270125	0.3523411	0.8661574
RED_72h_HW_S3	11192256	0.3577568	0.8669959
RED_d6_HW_S1	12601293	0.3594992	0.9232063
RED_d6_HW_S2	14389195	0.3773566	0.9008214
RED_d6_HW_S3	10369047	0.3596886	0.9337048
PLAS_5th_HW_S1	10464890	0.2979054	0.9197204
PLAS_5th_HW_S2	12413539	0.3516809	0.8726352
PLAS_5th_HW_S3	12144448	0.3412666	0.8815356
PLAS_72h_HW_S1	22056745	0.3432156	0.8879449
PLAS_72h_HW_S2	16270780	0.3781781	0.8736359
PLAS_72h_HW_S3	17941382	0.3628835	0.8848821
PLAS_d6_HW_S1	10272299	0.3684488	0.8459599
PLAS_d6_HW_S2	10360490	0.356322	0.8663535
PLAS_d6_HW_S3	10325251	0.3530437	0.8649025
PLAS_pp_HW_S1	11571587	0.3646058	0.9190389
PLAS_pp_HW_S2	12371662	0.3734378	0.90761
PLAS_pp_HW_S3	10198689	0.3560871	0.9288967

Table S7. RNA-seq library information and alignment rate.

Library name	Aligned reads	Alignment rate
RED_5th_HW_S1	29588544	84%
RED_5th_HW_S2	30910794	88%
RED_5th_HW_S3	29804252	83%
RED_pp_HW_S1	31669203	88%
RED_pp_HW_S2	28229472	87%
RED_pp_HW_S3	29412612	86%
RED_72h_HW_S1	30411621	89%
RED_72h_HW_S2	25236102	84%
RED_72h_HW_S3	32034233	88%
RED_d6_HW_S1	32380746	81%
RED_d6_HW_S2	27741489	86%
RED_d6_HW_S3	24542318	73%
PLAS_5th_HW_S1	28694536	83%
PLAS_5th_HW_S2	39499508	88%
PLAS_5th_HW_S3	26417448	85%
PLAS_72h_HW_S1	24745813	85%
PLAS_72h_HW_S2	35431663	88%
PLAS_72h_HW_S3	28534230	85%
PLAS_d6_HW_S1	23609699	84%
PLAS_d6_HW_S2	14505668	85%
PLAS_d6_HW_S3	28289401	82%
PLAS_pp_HW_S1	22913139	76%
PLAS_pp_HW_S2	25917156	74%
PLAS_pp_HW_S3	20730881	77%

Table S8. Hi-C library information.

Development stage	Sequenced reads	Alignable reads	Hi-C contacts	Pair type (L-I-O-R)
5th instar	653250687	492376131	196585889	25%-25%-25%-25%
72 hours	460369459	344078062	156321566	25%-25%-25%-25%

Development stage	Inter-scaffold	Intra-scaffold	Short-range	Long-range
5th instar	113429352	83156537	32287816	50868140
72 hours	82802944	73518622	41133097	32384920

Table S9. Hi-C looping interactions test results.

Loop interaction test results between a focal point and a CRE of interest. All Hi-C interaction tests were done using a Fisher's exact test. Peaks marked with an asterisk indicates variable accessibility between lines (Wald, adjusted p <0.05).

5th instar

Scaffold	Focus	CRE	Distance	*p*	Observed	Expected	ID
herfst							
000090F	66665	90641	23976	1.00	9	36.32	herfst_ATAC-peak-1
000090F	76795	90641	13846	1.00	15	48.74	herfst_ATAC-peak-2
000090F	109120	90641	-18479	0.57	17	16.85	herfst_ATAC-peak-3*
000090F	**119995**	**90641**	**-29354**	**5.78E-03**	**33**	**15.10**	**herfst_ATAC-peak-4***
000090F	**121275**	**90641**	**-30634**	**0.02**	**34**	**18.25**	**herfst_ATAC-peak-5***
herfst_ATAC_peak-3 interactions							
000090F	90641	109120	18479	0.87	17	22.81	herfst promotor
000090F	**121275**	**109120**	**-12155**	**0.00**	**90**	**38.56**	**herfst_ATAC-peak-5***
herfst_ATAC_peak-5 interactions							
000090F	**90641**	**121275**	**30634**	**4.05E-03**	**34**	**15.49**	**herfst promotor**
000090F	**109120**	**121275**	**12155**	**8.61E-04**	**90**	**53.19**	**herfst_ATAC-peak-3***
cortex							
000191F	**506210**	**409547**	**-96663**	**2.46E-03**	**40**	**17.54**	**cort_ATAC-peak-1**
000191F	**506434**	**409547**	**-96887**	**2.87E-03**	**41**	**18.92**	**cort_ATAC-peak-2**
000191F	511954	409547	-102407	5.05E-02	29	17.36	cort_ATAC-peak-3
000191F	512423	409547	-102876	9.80E-02	24	14.57	cort_ATAC-peak-4
000191F	**514864**	**409547**	**-105317**	**6.34E-03**	**40**	**20.14**	**cort_ATAC-peak-5**
000191F	**515524**	**409547**	**-105977**	**0.01**	**39**	**20.74**	**cort_ATAC-peak-6**
000191F	**516013**	**409547**	**-106466**	**8.84E-03**	**43**	**22.98**	**cort_ATAC-peak-7**
000191F	**517194**	**409547**	**-107647**	**0.03**	**42**	**25.76**	**cort_ATAC-peak-8**
000191F	**519013**	**409547**	**-109466**	**0.01**	**49**	**28.94**	**cort_ATAC-peak-9**

72 hours after pupation

herfst							
000090F	66665	90641	23976	0.99	17	31.23	herfst_ATAC-peak-1
000090F	76795	90641	13846	0.83	26	31.85	herfst_ATAC-peak-2
000090F	**109120**	**90641**	**-18479**	**4.73E-03**	**50**	**26.54**	**herfst_ATAC-peak-3***
000090F	**119995**	**90641**	**-29354**	**1.25E-06**	**47**	**11.52**	**herfst_ATAC-peak-4***

000090F	**121275**	**90641**	**-30634**	**3.53E-06**	**45**	**11.50**	**herfst_ATAC-peak-5***

herfst_ATAC_peak-3 interactions

000090F	**90641**	**109120**	**18479**	**1.25E-03**	**50**	**23.72**	**herfst promotor**
000090F	**121275**	**109120**	**-12155**	**2.88E-08**	**45**	**24.47**	**herfst_ATAC-peak-5***

herfst_ATAC_peak-5 interactions

000090F	**90641**	**121275**	**30634**	**4.57E-05**	**45**	**15.15**	**herfst promotor**
000090F	109120	121275	12155	0.11	75	59.58	herfst_ATAC-peak-3*

trehalase

000191F	775758	834187	58429	0.97	7	15.28	treh_ATAC-peak-1
000191F	**805440**	**834187**	**28747**	**4.99E-03**	**29**	**11.50**	**treh_ATAC-peak-2***
000191F	814090	834187	20097	0.20	14	8.70	treh_ATAC-peak-3
000191F	814480	834187	19707	0.06	19	9.91	treh_ATAC-peak-4

Table S10. CRISPR/Cas9 guides and genotyping primers.

Gene	gRNA	gRNA sequence
cortex	sgRNA_1	GGGCTGTTCCTGGGGTAATG
cortex	sgRNA_2	GCTGGAGTATATCTCCAGGG
cortex	sgRNA_3	TGTCGGACTCCAGTCGACAG
cortex	sgRNA_4	CCATGGCGCAGCGCGTTGCT
Dscam3	sgRNA_1	GGTGTGGGTGTCAGCGGGGG
Dscam3	sgRNA_2	GTTCAAGGCGGCCGTGGCGG
herfst	sgRNA_1	GGCTCTCCTTCTAGCTCTTC
herfst	sgRNA_2	CAAGAAGACACAATACACTT
herfst	sgRNA_3	GGGGTTGGTGCTGTATCATG
herfst	sgRNA_4	GACAAACAGTTCACTACTTC
trehalase	sgRNA_1	GGAATGAAAGACACAGTCAA
trehalase	sgRNA_2	GGTGGGACTTTTCTACGCGT
trehalase	sgRNA_3	TGGTAGATCCGCGTATACCA
trehalase	sgRNA_4	AATCTGGGGCACGTTCCAAA

Gene	Genotyping primer forward	Genotyping primer reverse
cortex 1+2	GGTTTGTGTCCCTGTCTGAA	CGTTGGATGGGAGCAGTTAT
cortex 3+4	TGGAGGTTCACAATAACAAGTTG	GGTCTCCCGCACCTTGGA
Dscam3	CCGTTCCGTAGCAGTGTTAAT	GTAAGCCGTGCACTGGTAG
herfst 1+2	CAGGCAAACAGCATTCAAAGT	CTCGTCATCAGACTCCAATTCC
herfst 3+4	ACAGAGAGTGGGAGAAACGA	TCCGACCACATAGAACACACT
trehalase 1+2	CGCCAAATGAACTCGAGAATTG	CATCCACAGTGGTGCTATGTTA
trehalase 1+2	TGTTGACCTCGAGATTTTAGTGG	ACCAATAGTCTAACTCTGCTTCG

Table S11. CRISPR injections, survival rate, and efficiency.

Gene	gRNA	sgRNA ng/µL	Cas9 ng/µL	Eggs injected	Hatched	%	Adults	%	Mutant phenotypes	%
cortex	1+2	130	100	958	52	5%	48	92%	4	8%
cortex	1+2	300	100	1101	229	21%	49	21%	0	0%
cortex	3+4	500	250	684	61	9%	35	57%	12	34%
cortex	1+2	1294	100	467	19	4%	6	32%	0	0%
Dscam3	1+2	130	100	761	34	4%	26	76%	0	0%
Dscam3	1+2	300	100	415	98	24%	49	50%	0	0%
Dscam3	1+2	430	100	179	16	9%	2	13%	0	0%
herfst	1+2	130	100	1112	46	4%	32	70%	2	6%
herfst	1+2	215	100	327	33	10%	17	52%	2	12%
herfst	1+2	300	100	496	156	31%	72	46%	12	17%
herfst	1+2	430	100	303	6	2%	3	50%	0	0%
herfst	3+4	500	250	404	117	29%	89	76%	6	7%
trehalase	1+2	130	100	972	72	7%	41	57%	5	12%
trehalase	1+2	215	100	500	205	41%	81	40%	6	7%
trehalase	1+2	300	100	1016	183	18%	127	69%	4	3%
trehalase	1+2	430	100	163	22	13%	12	55%	0	0%
trehalase	3+4	500	250	480	143	30%	82	57%	2	2%

Table S12. CRISPR/Cas9 mutant phenotypes.

	Red scales	Eyespot	Wing growth	No pigment	Reduced melanin / eyespot iridescence
herfst	4	3	6	6	
cortex	9	1	1	1	3
trehalase	2	4	5	5	

References

1. D. W. Pfennig, M. A. Wund, E. C. Snell-Rood, T. Cruickshank, C. D. Schlichting, A. P. Moczek, Phenotypic plasticity's impacts on diversification and speciation. *Trends Ecol. Evol.* **25**, 459–467 (2010). doi:10.1016/j.tree.2010.05.006 Medline

2. R. F. Schneider, A. Meyer, How plasticity, genetic assimilation and cryptic genetic variation may contribute to adaptive radiations. *Mol. Ecol.* **26**, 330–350 (2017). doi:10.1111/mec.13880 Medline

3. M. J. West-Eberhard, *Developmental Plasticity and Evolution* (Oxford Univ. Press, ed. 1, 2003).

4. C. H. Waddington, Genetic assimilation of an acquired character. *Evolution* **7**, 118–126 (1953). doi:10.1111/j.1558-5646.1953.tb00070.x

5. J.-M. Gibert, The flexible stem hypothesis: Evidence from genetic data. *Dev. Genes Evol.* **227**, 297–307 (2017). doi:10.1007/s00427-017-0589-0 Medline

6. K. C. Smith, The Effects of Temperature and Daylength on the Rosa Polyphenism in the Buckeye Butterfly, *Precis coenia* (Lepidoptera: Nymphalidae). *J. Res. Lepid.* **30**, 225–236 (1991).

7. D. B. Rountree, H. F. Nijhout, Genetic control of a seasonal morph in *Precis coenia* (Lepidoptera: Nymphalidae). *J. Insect Physiol.* **41**, 1141–1145 (1995). doi:10.1016/0022-1910(95)00051-U

8. E. V. Daniels, K. A. Mooney, R. D. Reed, Seasonal wing colour plasticity varies dramatically between buckeye butterfly populations in different climatic zones. *Ecol. Entomol.* **37**, 155–159 (2012). doi:10.1111/j.1365-2311.2012.01342.x

9. C. H. Waddington, Experiments on canalizing selection. *Genet. Res.* **1**, 140–150 (1960). doi:10.1017/S0016672300000136

10. H. F. Nijhout, Development and evolution of adaptive polyphenisms. *Evol. Dev.* **5**, 9–18 (2003). doi:10.1046/j.1525-142X.2003.03003.x Medline

11. D. B. Rountree, H. F. Nijhout, Hormonal control of a seasonal polyphenism in Precis coenia (Lepidoptera: Nymphalidae). *J. Insect Physiol.* **41**, 987–992 (1995). doi:10.1016/0022-1910(95)00046-W

12. N. J. Nadeau, C. Pardo-Diaz, A. Whibley, M. A. Supple, S. V. Saenko, R. W. R. Wallbank, G. C. Wu, L. Maroja, L. Ferguson, J. J. Hanly, H. Hines, C. Salazar, R. M. Merrill, A. J. Dowling, R. H. ffrench-Constant, V. Llaurens, M. Joron, W. O. McMillan, C. D. Jiggins, The gene cortex controls mimicry and crypsis in butterflies and moths. *Nature* **534**, 106–110 (2016). doi:10.1038/nature17961 Medline

13. A. E. Van't Hof, P. Campagne, D. J. Rigden, C. J. Yung, J. Lingley, M. A. Quail, N. Hall, A. C. Darby, I. J. Saccheri, The industrial melanism mutation in British peppered moths is a transposable element. *Nature* **534**, 102–105 (2016). doi:10.1038/nature17951 Medline

14. F. Figon, J. Casas, Ommochromes in invertebrates: Biochemistry and cell biology. *Biol. Rev. Camb. Philos. Soc.* **94**, 156–183 (2018). doi:10.1111/brv.12441 Medline

15. I. M. Ehrenreich, D. W. Pfennig, Genetic assimilation: A review of its potential proximate causes and evolutionary consequences. *Ann. Bot.* **117**, 769–779 (2016). doi:10.1093/aob/mcv130 Medline

16. J.-M. Belton, R. P. McCord, J. H. Gibcus, N. Naumova, Y. Zhan, J. Dekker, Hi-C: A comprehensive technique to capture the conformation of genomes. *Methods* **58**, 268–276 (2012). doi:10.1016/j.ymeth.2012.05.001 Medline

17. E. V. Daniels, R. Murad, A. Mortazavi, R. D. Reed, Extensive transcriptional response associated with seasonal plasticity of butterfly wing patterns. *Mol. Ecol.* **23**, 6123–6134 (2014). doi:10.1111/mec.12988 Medline

18. R. T. Yamamoto, Mass rearing of the tobacco hornworm. II. Larval rearing and pupation. *J. Econ. Entomol.* **62**, 1427–1431 (1969). doi:10.1093/jee/62.6.1427

19. H. F. Nijhout, Pattern formation on lepidopteran wings: Determination of an eyespot. *Dev. Biol.* **80**, 267–274 (1980). doi:10.1016/0012-1606(80)90403-0 Medline

20. V. Oostra, M. A. de Jong, B. M. Invergo, F. Kesbeke, F. Wende, P. M. Brakefield, B. J. Zwaan, Translating environmental gradients into discontinuous reaction norms via hormone signalling in a polyphenic butterfly. *Proc. R. Soc. B* **278**, 789–797 (2011). doi:10.1098/rspb.2010.1560

21. J. R. G. Turner, P. M. Sheppard, Absence of crossing-over in female butterflies (*Heliconius*). *Heredity* **34**, 265–269 (1975). doi:10.1038/hdy.1975.29 Medline

22. M. Martin, Cutadapt removes adapter sequences from high-throughput sequencing reads. *EMBnet J.* **17**, 10 (2011). doi:10.14806/ej.17.1.200

23. K. R. L. van der Burg, J. J. Lewis, A. Martin, H. F. Nijhout, C. G. Danko, R. D. Reed, Contrasting roles of transcription factors Spineless and EcR in the highly dynamic chromatin landscape of butterfly wing metamorphosis. *Cell Rep.* **27**, 1027–1038.e3 (2019). doi:10.1016/j.celrep.2019.03.092 Medline

24. B. Langmead, S. L. Salzberg, Fast gapped-read alignment with Bowtie 2. *Nat. Methods* **9**, 357–359 (2012). doi:10.1038/nmeth.1923 Medline

25. A. McKenna, M. Hanna, E. Banks, A. Sivachenko, K. Cibulskis, A. Kernytsky, K. Garimella, D. Altshuler, S. Gabriel, M. Daly, M. A. DePristo, The Genome Analysis Toolkit: A MapReduce framework for analyzing next-generation DNA sequencing data. *Genome Res.* **20**, 1297–1303 (2010). doi:10.1101/gr.107524.110 Medline

26. S. Purcell, B. Neale, K. Todd-Brown, L. Thomas, M. A. R. Ferreira, D. Bender, J. Maller, P. Sklar, P. I. W. de Bakker, M. J. Daly, P. C. Sham, PLINK: A tool set for whole-genome association and population-based linkage analyses. *Am. J. Hum. Genet.* **81**, 559–575 (2007). doi:10.1086/519795 Medline

27. J. Buenrostro, B. Wu, H. Chang, W. Greenleaf, *Curr. Protoc. Mol. Biol.* **109**, 21.29.1–21.29.9 (2015).

28. J. J. Lewis, R. C. Geltman, P. C. Pollak, K. E. Rondem, S. M. Van Belleghem, M. J. Hubisz, P. R. Munn, L. Zhang, C. Benson, A. Mazo-Vargas, C. G. Danko, B. A. Counterman, R. Papa, R. D. Reed, Parallel evolution of ancient, pleiotropic enhancers underlies butterfly wing pattern mimicry. *Proc. Natl. Acad. Sci. U.S.A.* **116**, 24174–24183 (2019). doi:10.1073/pnas.1907068116 Medline

29. J. J. Lewis, R. D. Reed, Genome-wide regulatory adaptation shapes population-level genomic landscapes in *Heliconius*. *Mol. Biol. Evol.* **36**, 159–173 (2019). doi:10.1093/molbev/msy209 Medline

30. M. I. Love, W. Huber, S. Anders, Moderated estimation of fold change and dispersion for RNA-seq data with DESeq2. *Genome Biol.* **15**, 550 (2014). doi:10.1186/s13059-014-0550-8 Medline

31. F. Ramírez, D. P. Ryan, B. Grüning, V. Bhardwaj, F. Kilpert, A. S. Richter, S. Heyne, F. Dündar, T. Manke, deepTools2: A next generation web server for deep-sequencing data analysis. *Nucleic Acids Res.* **44**, W160–W165 (2016). doi:10.1093/nar/gkw257 Medline

32. A. P. Boyle, J. Guinney, G. E. Crawford, T. S. Furey, F-Seq: A feature density estimator for high-throughput sequence tags. *Bioinformatics* **24**, 2537–2538 (2008). doi:10.1093/bioinformatics/btn480 Medline

33. S. S. P. Rao, M. H. Huntley, N. C. Durand, E. K. Stamenova, I. D. Bochkov, J. T. Robinson, A. L. Sanborn, I. Machol, A. D. Omer, E. S. Lander, E. L. Aiden, A 3D map of the human genome at kilobase resolution reveals principles of chromatin looping. *Cell* **159**, 1665–1680 (2014). doi:10.1016/j.cell.2014.11.021 Medline

34. J. Ray, P. R. Munn, A. Vihervaara, J. J. Lewis, A. Ozer, C. G. Danko, J. T. Lis, Chromatin conformation remains stable upon extensive transcriptional changes driven by heat shock. *Proc. Natl. Acad. Sci. U.S.A.* **116**, 19431–19439 (2019). doi:10.1073/pnas.1901244116 Medline

35. N. C. Durand, M. S. Shamim, I. Machol, S. S. P. Rao, M. H. Huntley, E. S. Lander, E. L. Aiden, Juicer provides a one-click system for analyzing loop-resolution Hi-C experiments. *Cell Syst.* **3**, 95–98 (2016). doi:10.1016/j.cels.2016.07.002 Medline

36. J. J. Lewis, S. M. Van Belleghem, R. Papa, C. G. Danko, R. D. Reed, Many functionally connected loci foster adaptive diversification along a neotropical hybrid zone. *Sci. Adv.* **6**, eabb8617 (2020). doi:10.1126/sciadv.abb8617 Medline

37. J. W. Davey, M. Chouteau, S. L. Barker, L. Maroja, S. W. Baxter, F. Simpson, R. M. Merrill, M. Joron, J. Mallet, K. K. Dasmahapatra, C. D. Jiggins, Major improvements to the *Heliconius melpomene* genome assembly used to confirm 10 chromosome fusion events in 6 million years of butterfly evolution. *G3* **6**, 695–708 (2016). Medline

38. L. Zhang, A. Martin, M. W. Perry, K. R. L. van der Burg, Y. Matsuoka, A. Monteiro, R. D. Reed, Genetic basis of melanin pigmentation in butterfly wings. *Genetics* **205**, 1537–1550 (2017). doi:10.1534/genetics.116.196451 Medline

39. E. K. Brinkman, T. Chen, M. Amendola, B. van Steensel, Easy quantitative assessment of genome editing by sequence trace decomposition. *Nucleic Acids Res.* **42**, e168–e168 (2014). doi:10.1093/nar/gku936 Medline